Molecular Simulation of Liquid Crystals

Mike Allen

Centre for Scientific Computing and Department of Physics,
University of Warwick, Coventry CV4 7AL, United Kingdom

m.p.allen@warwick.ac.uk

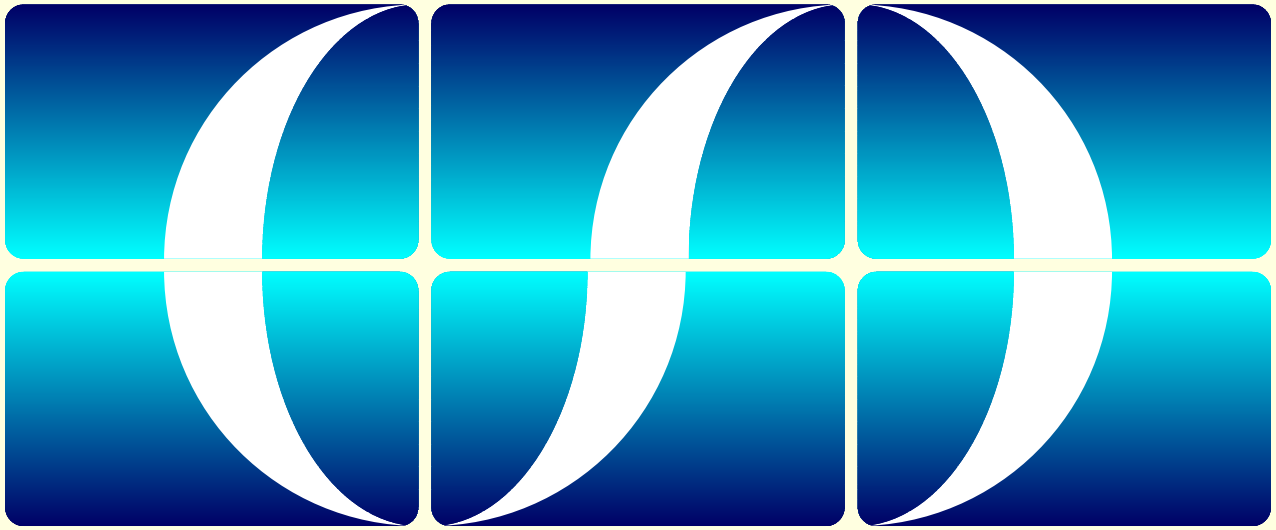

Isotropic Liquid Phase

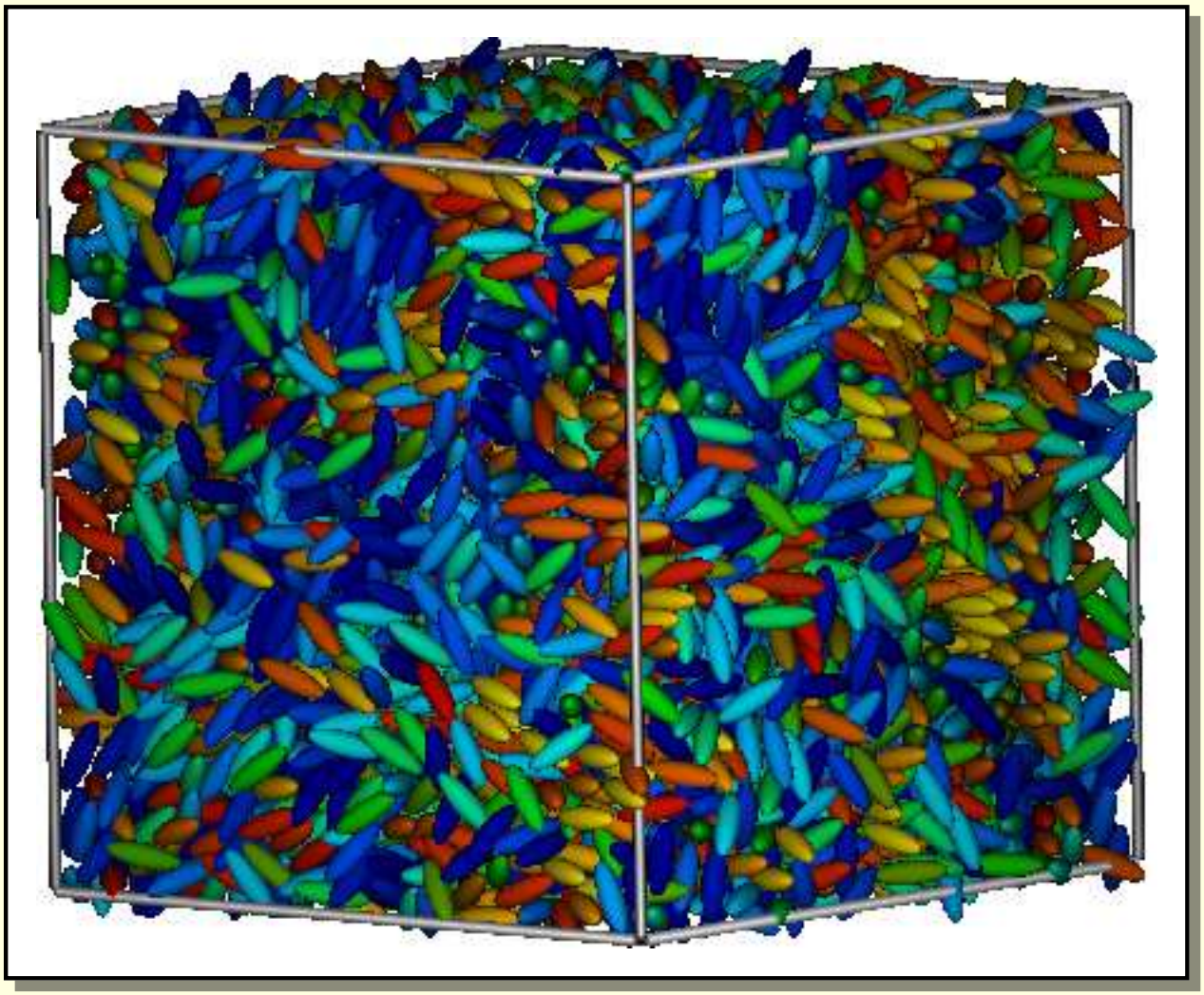

Nematic Liquid Crystal Phase

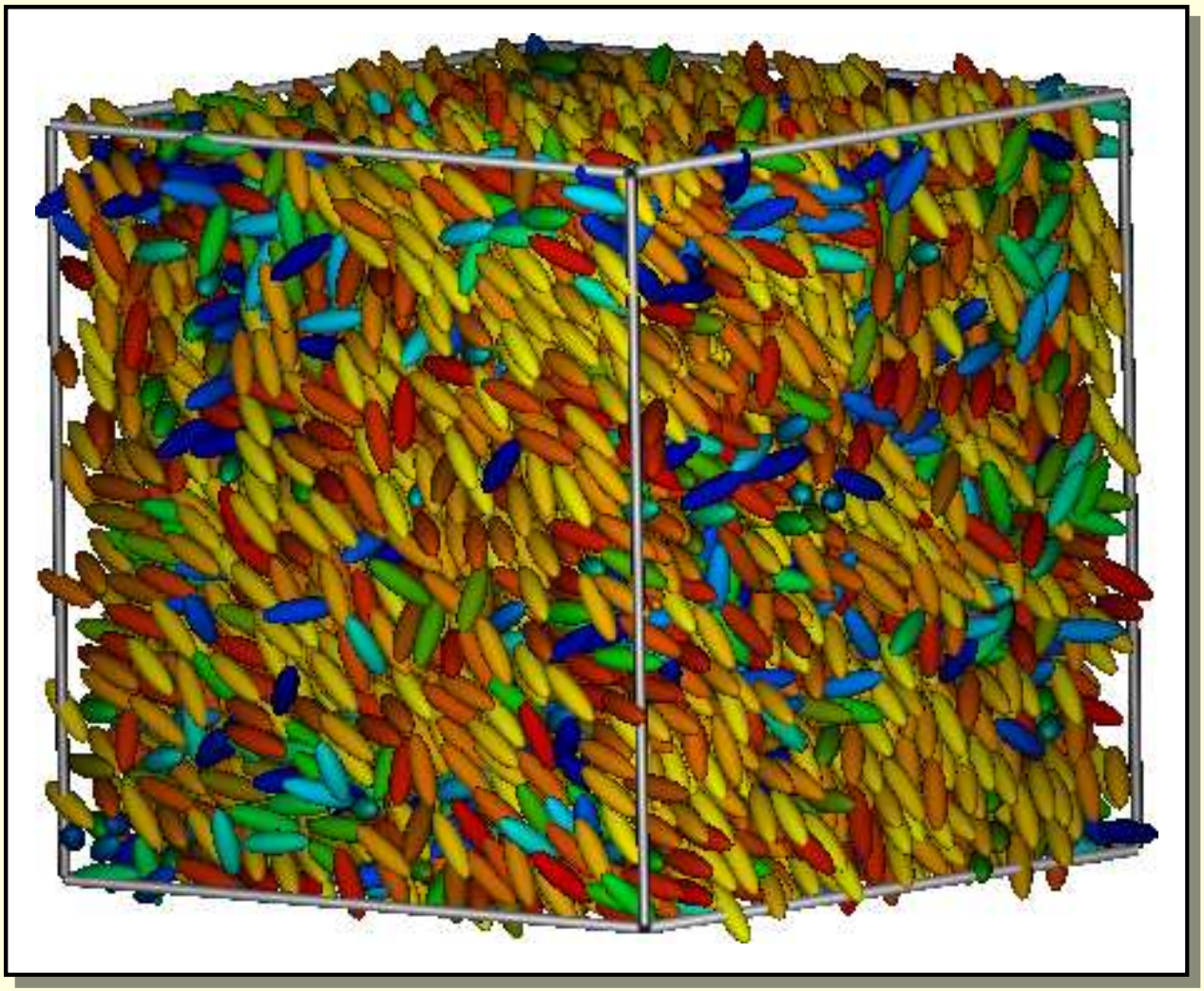

Smectic-A Liquid Crystal Phase

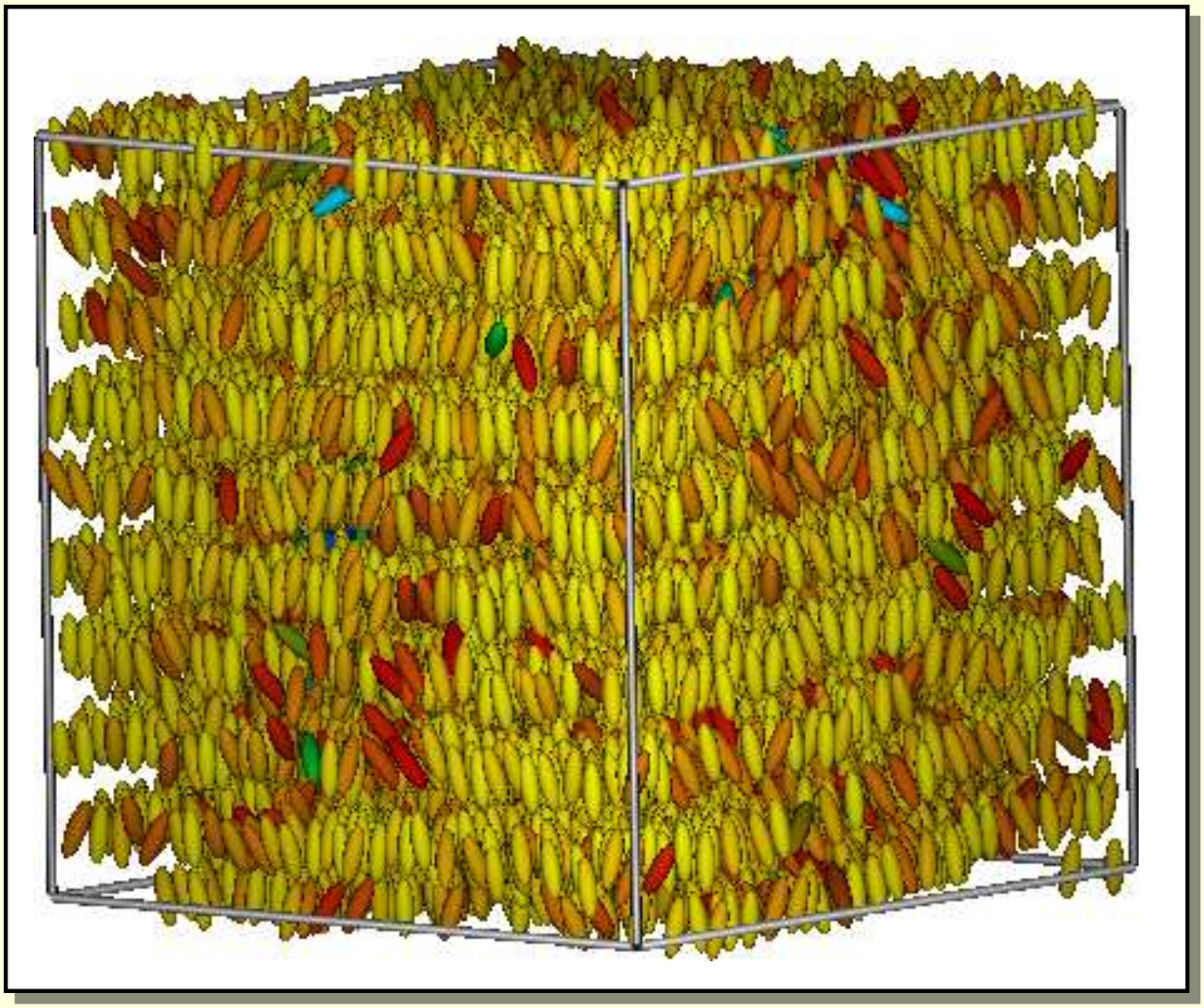

Example Results: rod-plate mixtures

Left: isotropic (I) phase for $e = 20, 1/20$ mixture.

Right: nematic (N_+) phase for $e = 20, 1/20$ mixture.

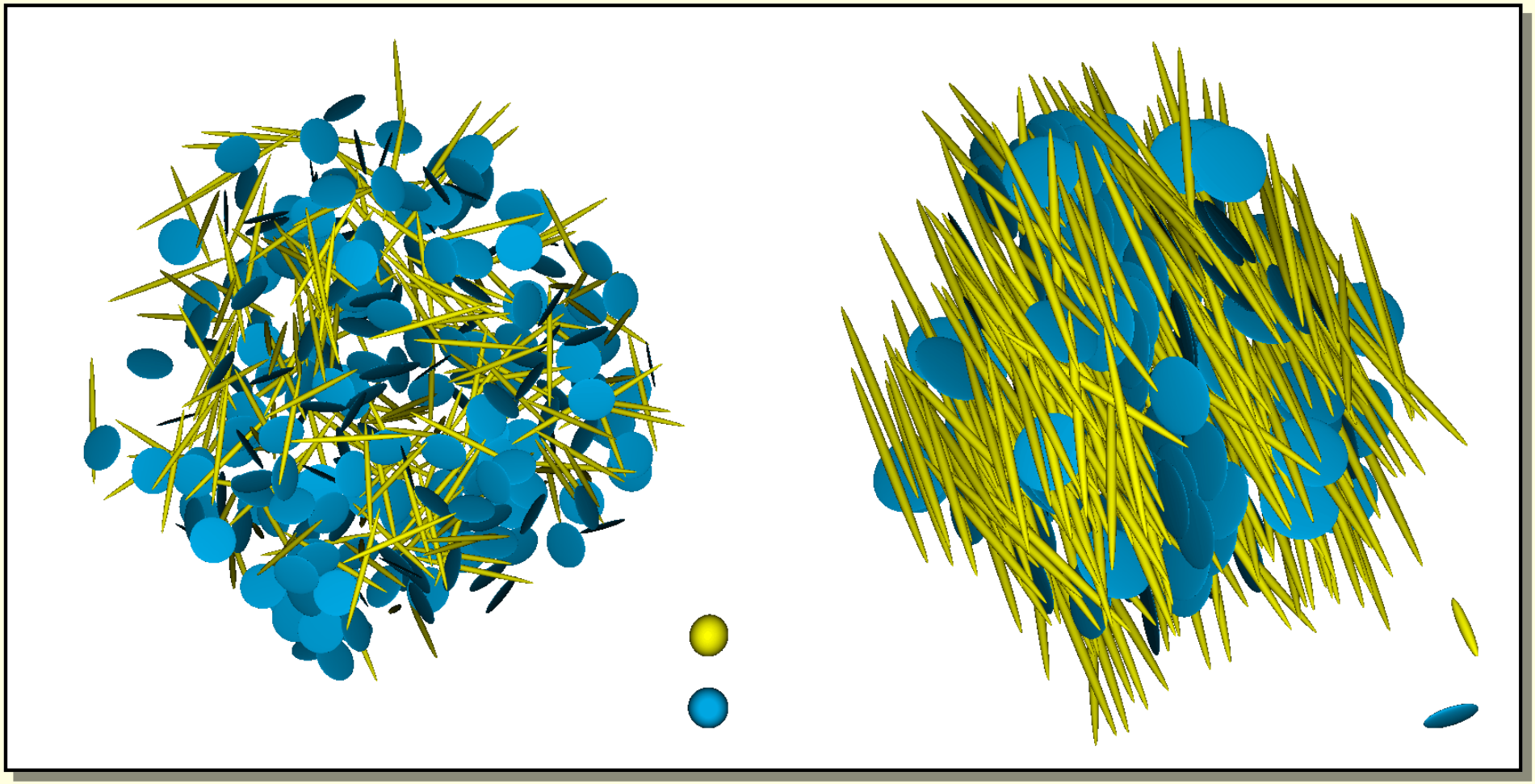

Example Results: rod-plate mixtures

Left: nematic (N_-) phase for $e = 20, 1/20$ mixture. Right: biaxial (B) phase, but with demixing, for $e = 20, 1/20$ mixture.

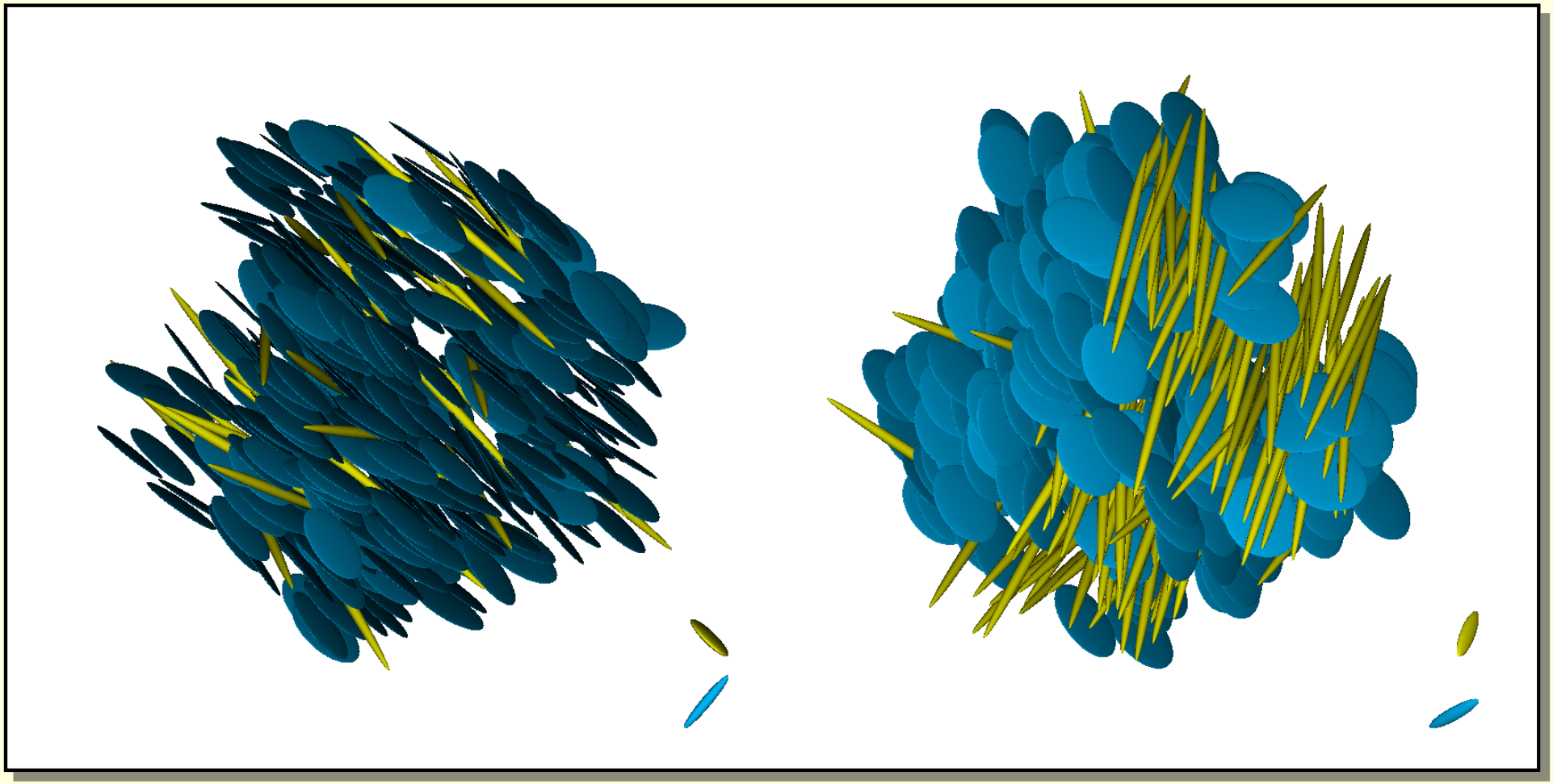

Example Results: rod-plate mixtures

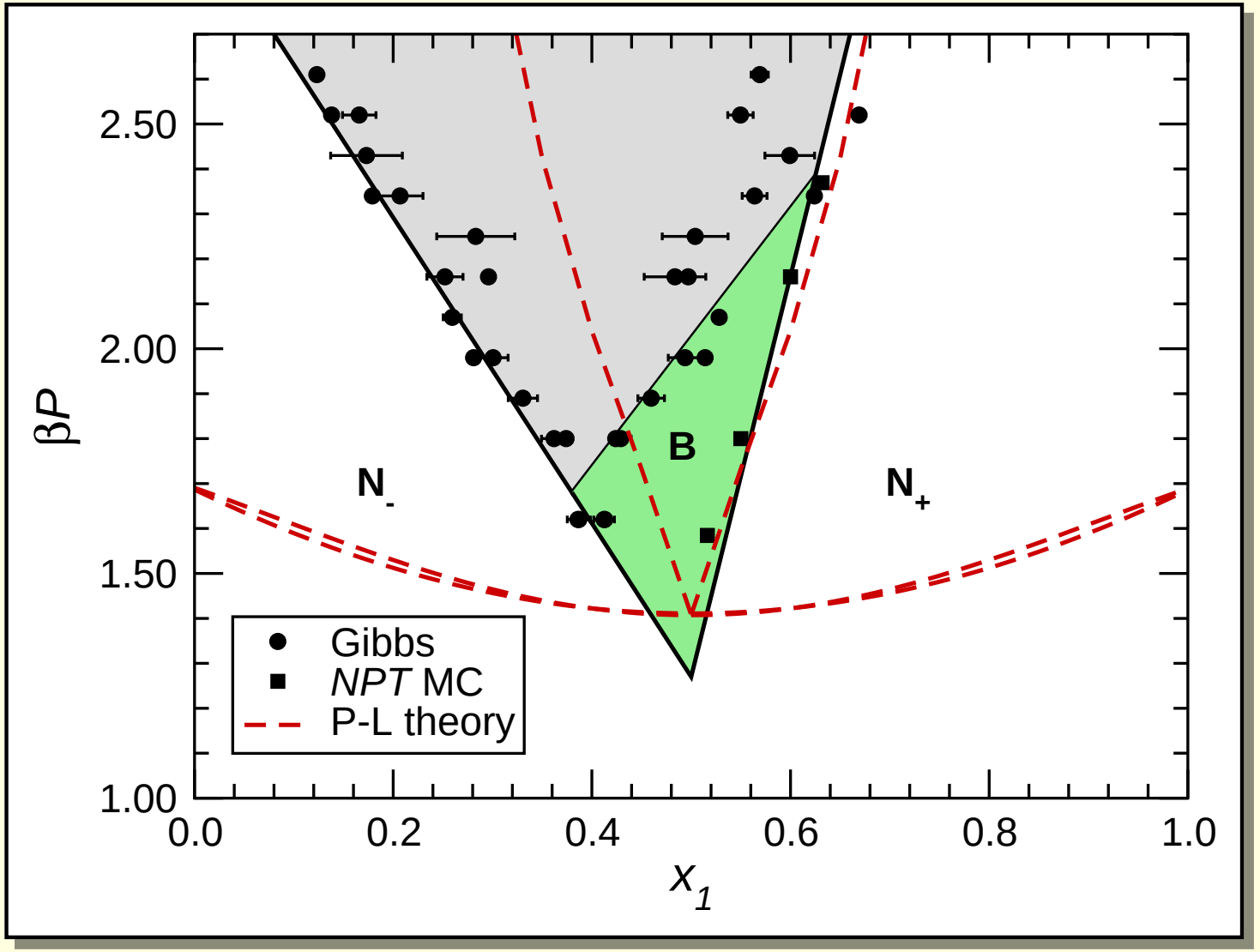

Camp, MPA, Bolhuis, Frenkel, *J. Chem. Phys.*, **106,** 9270 (1997)

Where can simulation contribute?

- Computer simulation + liquid-state theories = insight.
- Molecular structure → liquid crystalline (LC) behaviour.
- Complements experimental synthesis and characterization.
- *BUT:* LC properties very sensitive to molecular details.
  - ↪ simulation faces a tough challenge.

Where can simulation contribute?

- Testing continuum theories of liquid crystals:
  - density-functional theories;
  - Landau-de Gennes theories;
  - elastic theories;
  - hydrodynamics.
- Computing phenomenological coefficients for the above theories and linking them with molecular structure.
- Describing molecular-scale effects, behaviour near surfaces and defects, which cannot be modelled properly in the continuum picture.

Molecular Models

- For specific experimental systems:
  - atomic detail, empirical potentials [1, 2];
  - and/or *ab initio* calculations [3, 4, 5];
- For more generic behaviour and method development
  - coarse-grained molecular models

We shall concentrate on the latter: but realistic modelling is no longer beyond the range of laboratory computers.

Coarse-grained modelling

Basic shapes: describe the basic nematic, smectic, etc. liquid crystals

- *ellipsoids of revolution* of length A, width B;
- *spherocylinders* of overall length $L + D$, width D.

Additional contributions:

- attractive forces [6, 7, 8, 9, 10];
- biaxiality [11, 12], nonlinearity [13];
- flexibility [14, 15];
- dipolar forces [16];
- hydrogen bonds [17].

Theoretical Approaches

Unifying feature: approximate free energy *functional* of simple functions of particle positions and orientations, e.g.

- the local single-particle density,
- the orientational order tensor,
- the direction of orientational ordering.

Variational problem: minimize the free energy with respect to all possible variations of these functions.

Oseen-Frank elastic theory

The Oseen-Frank [18, 19] free energy $\mathcal{F}_{\rm OF}$ is a functional of the position-dependent liquid crystal director $\boldsymbol{n}(\boldsymbol{r})$:

$$\mathcal{F}_{\rm OF}\left[\boldsymbol{n}(\boldsymbol{r})\right] = \int_V {\rm d}^3\boldsymbol{r}\; f_b(\boldsymbol{r}) + \int_S {\rm d}^2\boldsymbol{s}\; f_s(\boldsymbol{s})$$

$$f_b(\boldsymbol{r}) = \tfrac{1}{2}K_{11}\left(\nabla\cdot\boldsymbol{n}\right)^2 + \tfrac{1}{2}K_{22}\left(\boldsymbol{n}\cdot\nabla\times\boldsymbol{n}\right)^2 + \tfrac{1}{2}K_{33}\left(\boldsymbol{n}\times\nabla\times\boldsymbol{n}\right)^2$$

$$f_s(\boldsymbol{s}) = \tfrac{1}{2}W_\theta \sin^2\theta \quad \text{where } \cos\theta = \boldsymbol{n}\cdot\boldsymbol{n}_s \; .$$

- an integral, over sample volume V, of a bulk free energy density
  - splay (K_{11}), twist (K_{22}), bend (K_{33}) elastic constants.
- an integral, over surface S, of a surface free energy density
  - surface anchoring strength W_θ, preferred orientation $\boldsymbol{n}_s$.

Landau - de Gennes theory

The Landau and de Gennes [20] free energy $\mathcal{F}_{\mathrm{LdG}}$ is based on the 2^{nd}-rank order tensor $\mathbf{Q}(\boldsymbol{r})$:

$$\mathcal{F}_{\mathrm{LdG}}[\mathbf{Q}(\boldsymbol{r})] = \int_V \mathrm{d}^3\boldsymbol{r}\; f_b(\boldsymbol{r}) + \int_S \mathrm{d}^2\boldsymbol{s}\; f_s(\boldsymbol{s})$$

$$f_b(\boldsymbol{r}) = \kappa\left|\nabla\mathbf{Q}\right|^2 + a\mathrm{Tr}\left[\mathbf{Q}^2\right] - b\mathrm{Tr}\left[\mathbf{Q}^3\right] + c\left\{\mathrm{Tr}\left[\mathbf{Q}^2\right]\right\}^2$$

$$f_s(\boldsymbol{s}) = w\mathrm{Tr}\left[\mathbf{Q}-\mathbf{Q}_s\right]^2$$

- One-constant elastic behaviour (the squared gradient term);
- Leading terms in a free energy expansion, which would give a phenomenological description of the bulk I-N transition;
- Surface anchoring term, involving the preferred order tensor $\mathbf{Q}_s$ at the surface.

Onsager theory

The Onsager [21] free energy $\mathcal{F}_{\rm Ons}$ depends on the single-particle density $\varrho(\boldsymbol{A})$, where $\boldsymbol{A}$ represents position *and* orientation

$$\mathcal{F}_{\rm Ons}[\varrho(\boldsymbol{A})] = k_{\rm B}T \int {\rm d}\boldsymbol{A}\, \varrho(\boldsymbol{A}) \left[\ln \varrho(\boldsymbol{A})\Lambda^3 - 1 + u(\boldsymbol{A})/k_{\rm B}T \right]$$

$$- \tfrac{1}{2} k_{\rm B}T \iint {\rm d}\boldsymbol{A}\, {\rm d}\boldsymbol{B}\, \varrho(\boldsymbol{A})\varrho(\boldsymbol{B})\, f(\boldsymbol{A},\boldsymbol{B})$$

- Single particle entropy of mixing plus external field $u(\boldsymbol{A})$.
- The Mayer function $f(\boldsymbol{A},\boldsymbol{B}) = {\rm e}^{-v(\boldsymbol{A},\boldsymbol{B})/k_{\rm B}T} - 1$ is related directly to the intermolecular pair potential $v(\boldsymbol{A},\boldsymbol{B})$.

Onsager theory

- Forerunner of modern density functional theories [22, 23, 24, 25].
- Above expression is only valid for low densities, but is *not* restricted to smooth variations of $\varrho(\boldsymbol{A})$
  - ↪ which would lead to a gradient expansion
- May be (empirically) extended to higher densities [26, 27, 28].

Bulk elastic constants

Long-wavelength deformations of the director field $\boldsymbol{n}(\boldsymbol{r})$ are described by the Oseen-Frank free energy $\mathcal{F}_{\mathrm{OF}}$. Simulation can provide values of the coefficients K_1, K_2, K_3 in this expression. Define

$$Q_{\alpha\beta}(\boldsymbol{k},t) = \sum_i \left(\frac{3}{2} u_{i\alpha}(t) u_{i\beta}(t) - \frac{1}{2}\delta_{\alpha\beta} \right) \mathrm{e}^{\mathrm{i}\boldsymbol{k}\cdot\boldsymbol{r}_i(t)} \qquad \alpha,\beta = x,y,z$$

and choose coordinates so that $\boldsymbol{n}(\boldsymbol{r}) = (0,0,1)$, and $\boldsymbol{k} = (k_1,0,k_3)$. Then $\delta Q_{13} \propto \delta n_1$, $\delta Q_{23} \propto \delta n_2$, and

$$\mathcal{W}_{13}(k_1,k_3) \propto \langle |\hat{Q}_{13}(\boldsymbol{k})|^2 \rangle^{-1} \propto K_1 k_1^2 + K_3 k_3^2$$

$$\mathcal{W}_{23}(k_1,k_3) \propto \langle |\hat{Q}_{23}(\boldsymbol{k})|^2 \rangle^{-1} \propto K_2 k_1^2 + K_3 k_3^2$$

Bulk elastic constants

Gay-Berne potential, $\kappa = 3$, $\kappa' = 5$:

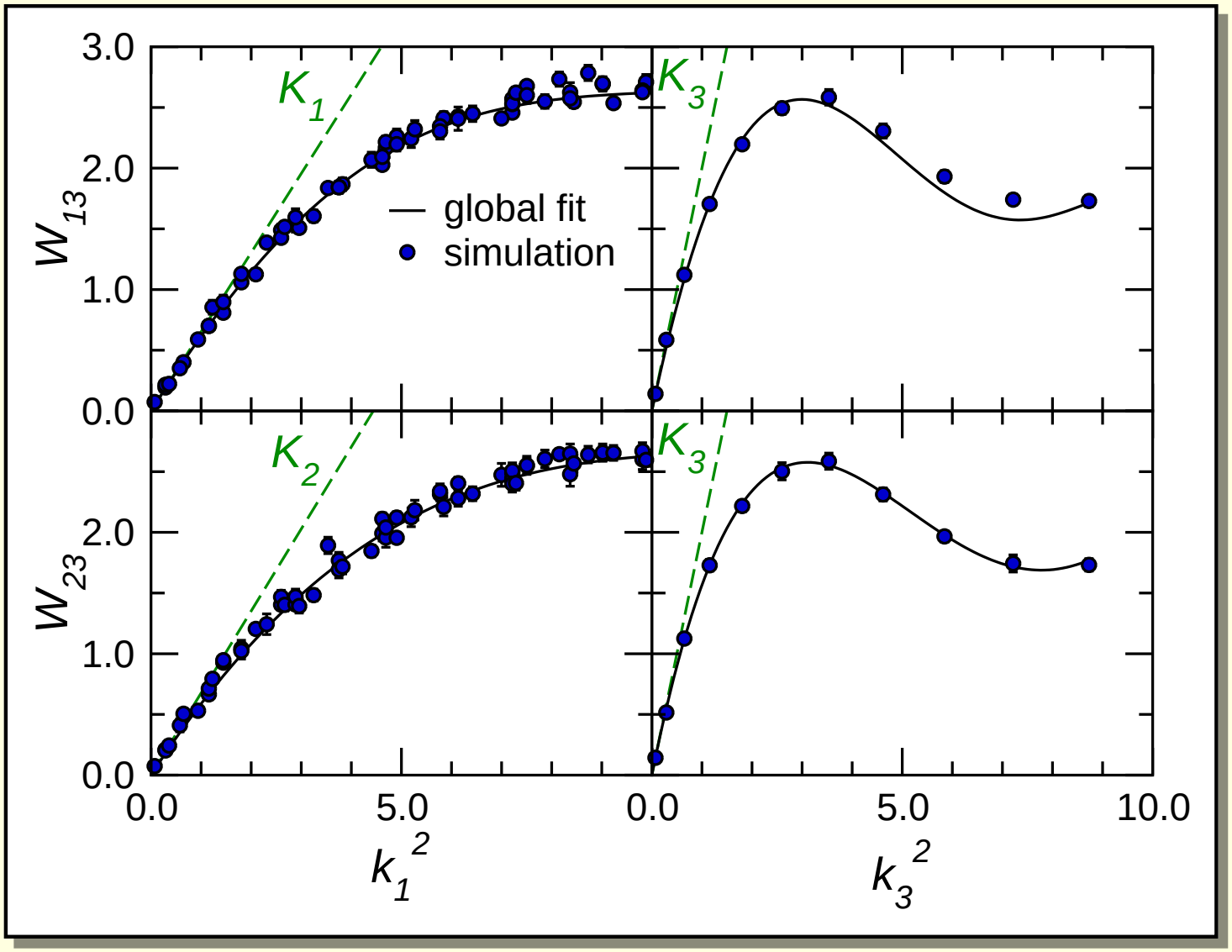

MPA, Warren, Wilson, Sauron, Smith, *J. Chem. Phys.*, **105,** 2850 (1996)

Anchoring and interfaces

Nematic-solid interface

- anchoring technology;
- theoretically subtle;
- computationally tough.

Nematic-isotropic interface

- simple fluid-fluid interface;
- interesting basic questions;
- simulate with great care.

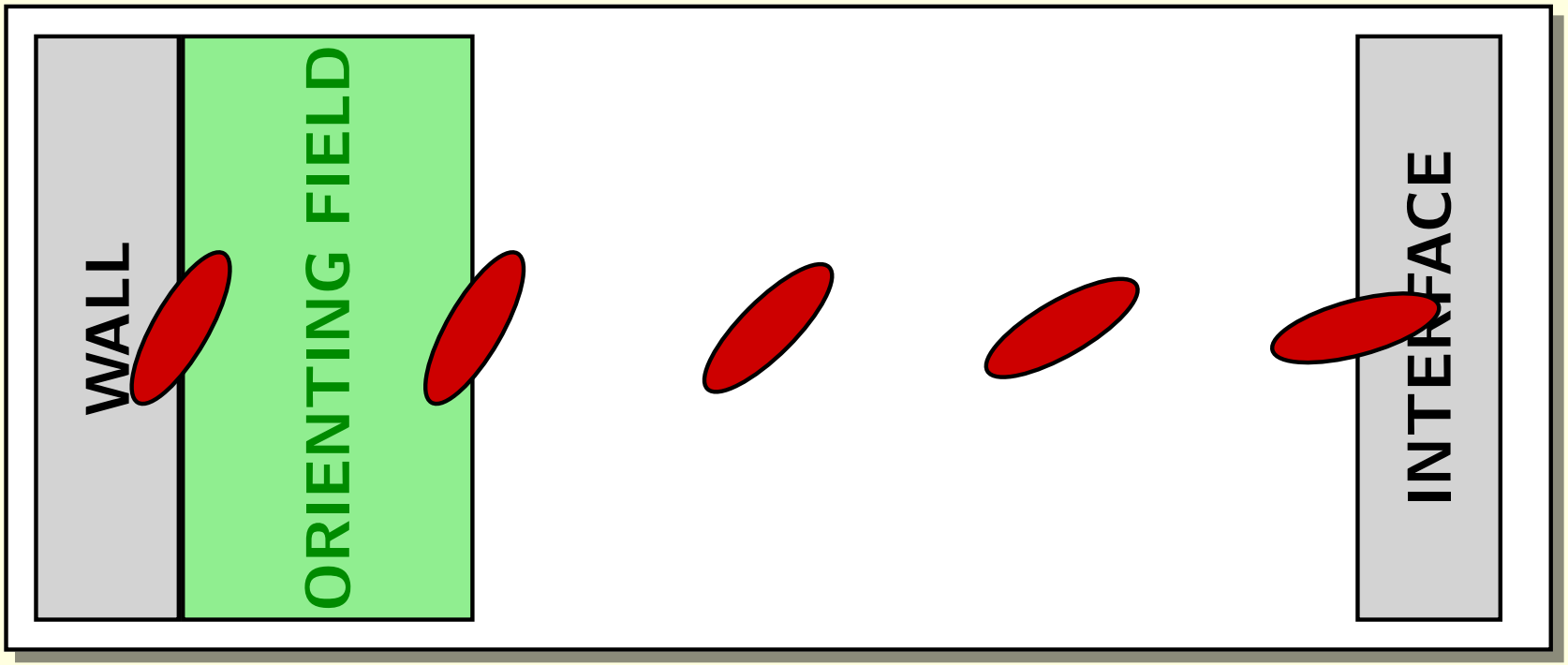

Surface anchoring

Surface anchoring coefficient:

W measures resistance of surface to director deformation.

Extrapolation length:

$\lambda = K_{33}/W$ by fitting director profiles to elastic theory.

Results:

- Elastic theory fits quite well, except near the walls.
- Extrapolation length λ is of order one molecular length.

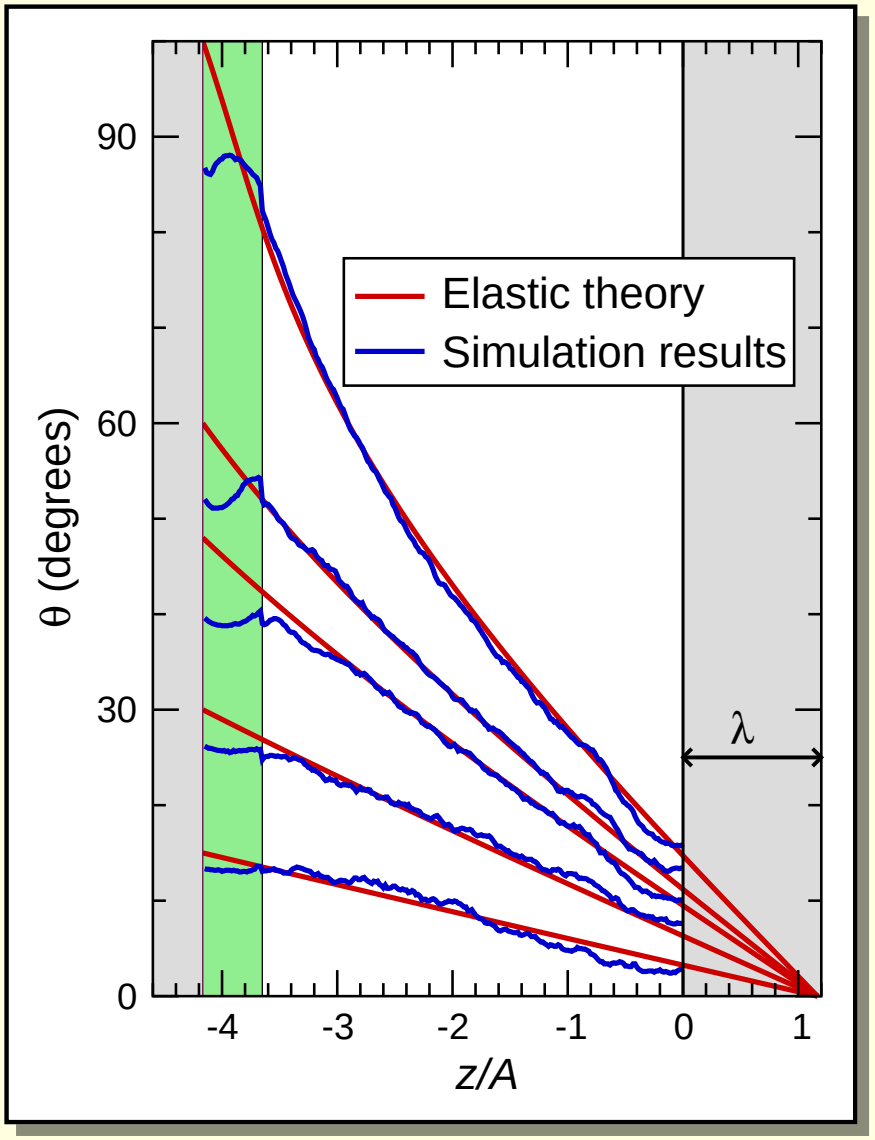

Onsager Theory

Direct minimization of the Onsager free energy functional, with essentially no adjustable parameters, reproduces these director profiles very well, *even in the wall regions where the elastic theory is inaccurate.*

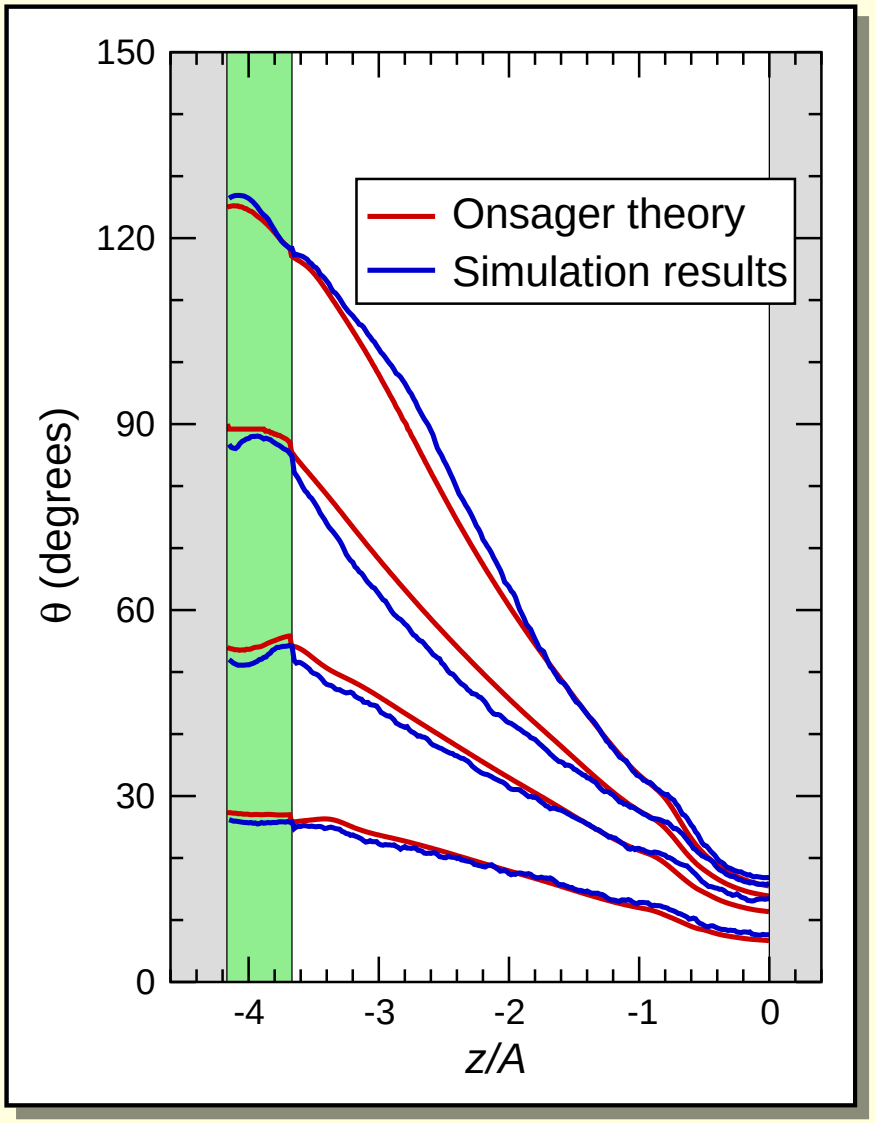

MPA, *Molec. Phys.*, **96,** 1391 (1999)

Fluctuations in confined geometry

- Large length- and time-scale fluctuations of the director $\boldsymbol{n}(\boldsymbol{r})$ can also be described by the phenomenological elastic theory.
- In slab geometry, fluctuation amplitudes can be expanded:

$$\delta\boldsymbol{n}(\boldsymbol{r}) \propto \sum_{\boldsymbol{q}_\perp, q_z} \mathrm{e}^{\mathrm{i}\boldsymbol{q}_\perp\cdot\boldsymbol{r}_\perp}\left[\delta\boldsymbol{n}^{(+)}(\boldsymbol{q}_\perp, q_z)\mathrm{e}^{\mathrm{i}q_z r_z} + \delta\boldsymbol{n}^{(-)}(\boldsymbol{q}_\perp, q_z)\mathrm{e}^{-\mathrm{i}q_z r_z}\right],$$

- This is parametrized by the dimensionless quantities

$$\chi = q_z L\,; \quad \xi = WL/K = L/\lambda\,; \quad \lambda = \text{extrapolation length.}$$

- Confinement in the z direction, with finite anchoring energy W, gives an *uneven* discrete spectrum q_z.
- In simulations, measure $Q_{\alpha z}(\boldsymbol{r}) \propto \delta n_\alpha(\boldsymbol{r})$

Molecular simulations

- Monte Carlo of hard ellipsoids, $A/B = 15$ between two hard parallel confining walls.
- Homeotropic anchoring.
- Wall separations: $L_z/A = 3.29, 4.11, 4.93$.

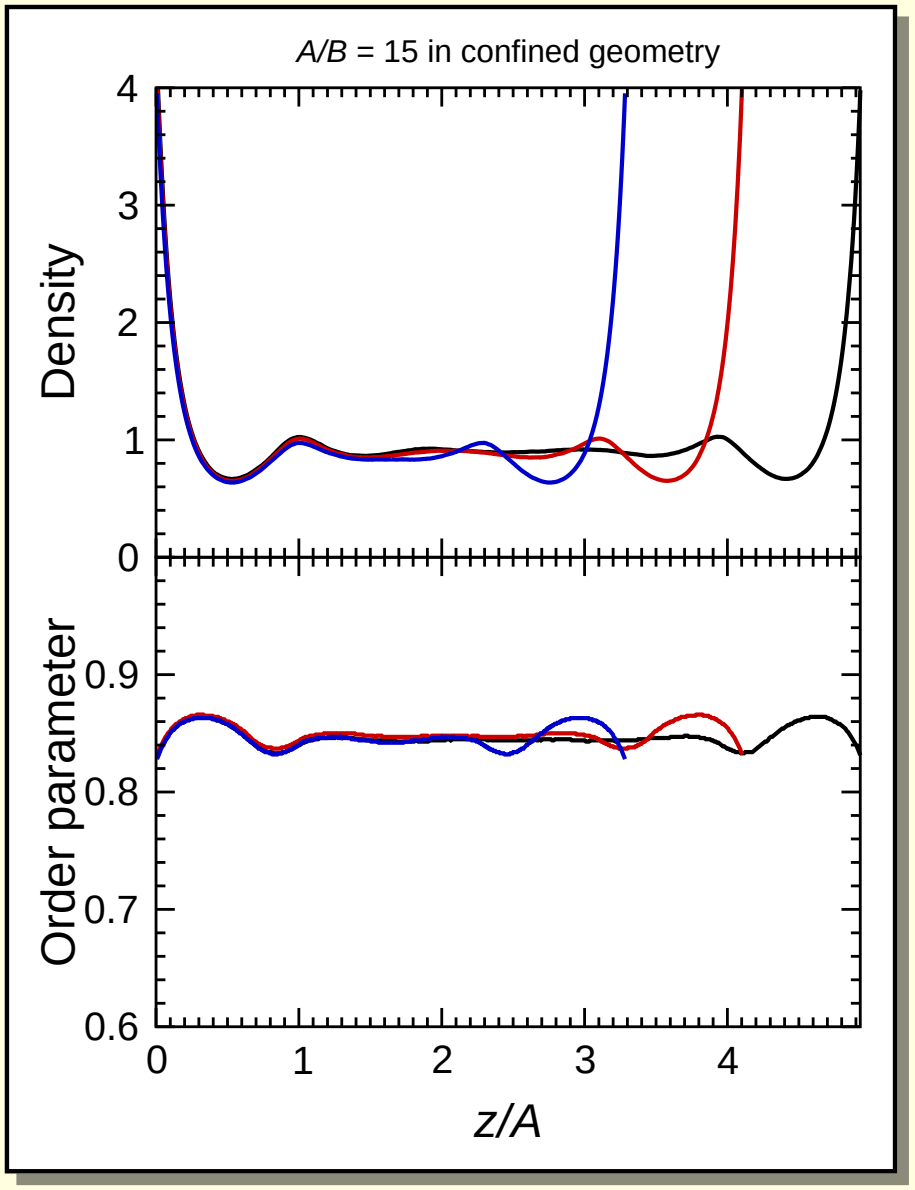

Elastic boundary position

Where is it correct to place the elastic boundary?

- $L = L_z + 2L_w$.
- L_w
  - characterizes wall;
  - independent of L_z.

Test the ratios

$$\frac{\left\langle |Q_{\alpha z}(L_z)|^2 \right\rangle}{\left\langle |Q_{\alpha z}(L_z')|^2 \right\rangle}$$

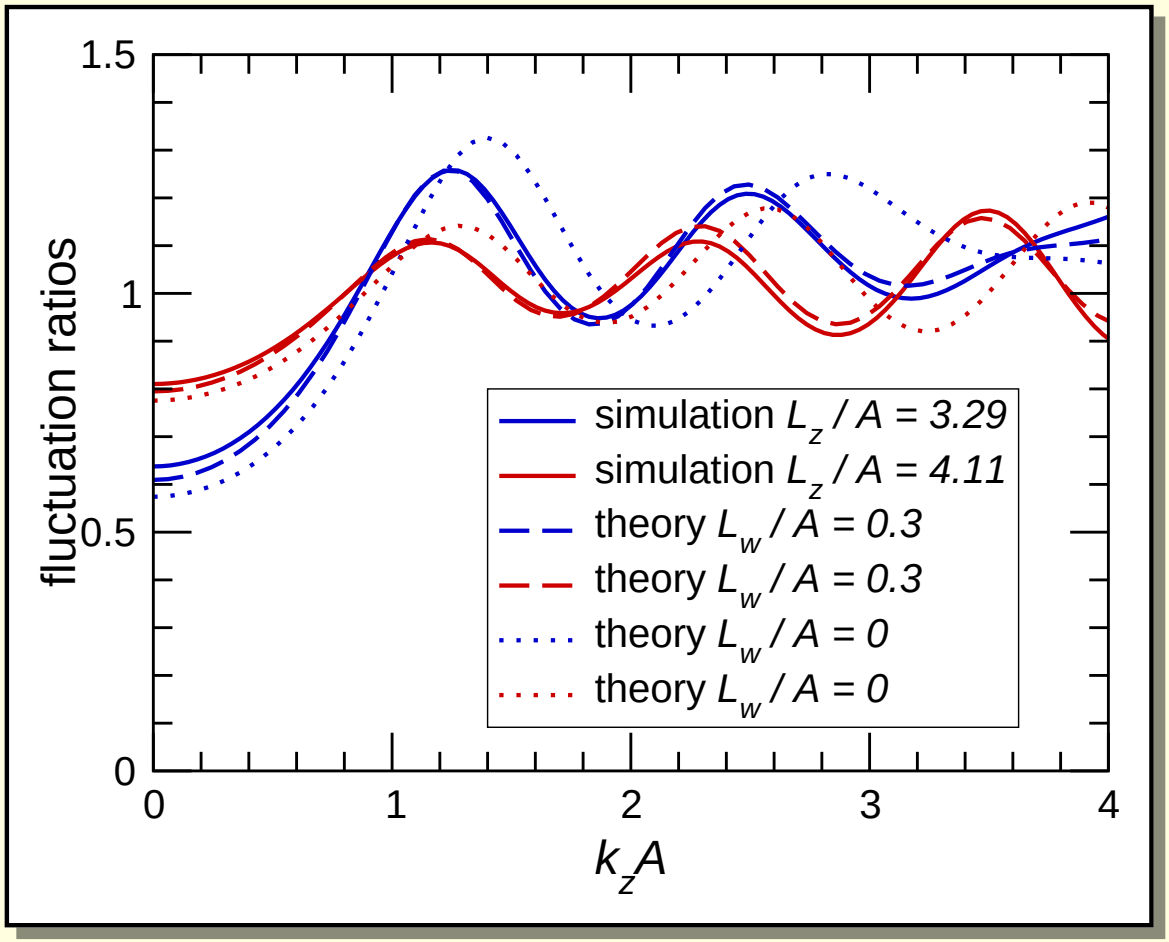

Anchoring variation with order parameter

Expected behaviour:

- $\lambda \propto Q^{-2}$.
- $K \propto Q^{2}$.
- Hence $W \propto Q^{4}$.

Surprise! With changing density and Q, the structure of the surface layer changes.

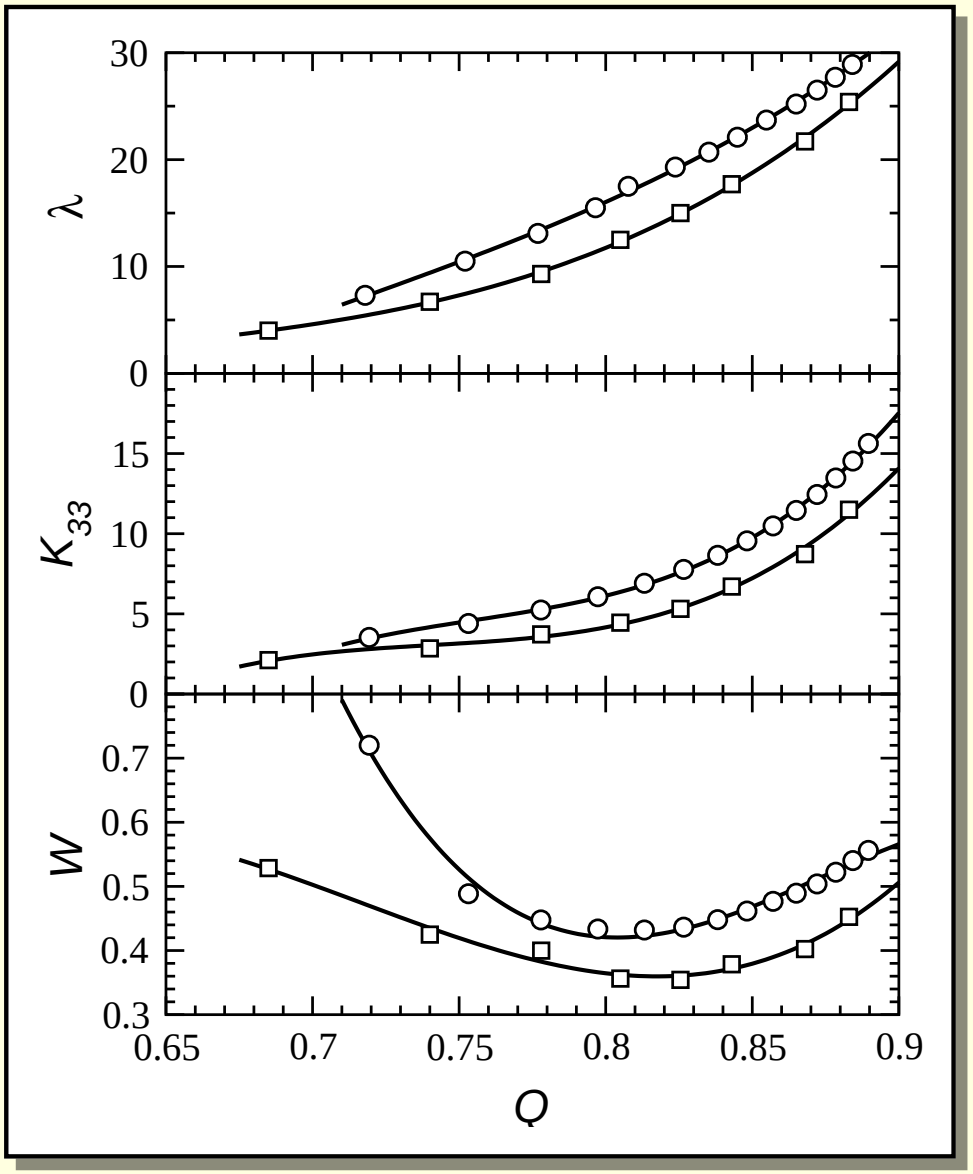

Nematic-Isotropic Interface

Nematic and isotropic phases *in coexistence*, at a solid wall, $A/B = 15$. We see *nematic wetting:* a thick film of nematic is adsorbed, with various specified anchoring conditions, here in the plane of the interface.

order parameter: λ_+;

scaled number density: $\rho A^2 B$;

film thickness: determined by distance from coexistence $\mu - \mu_{\mathrm{IN}}$ or total number N.

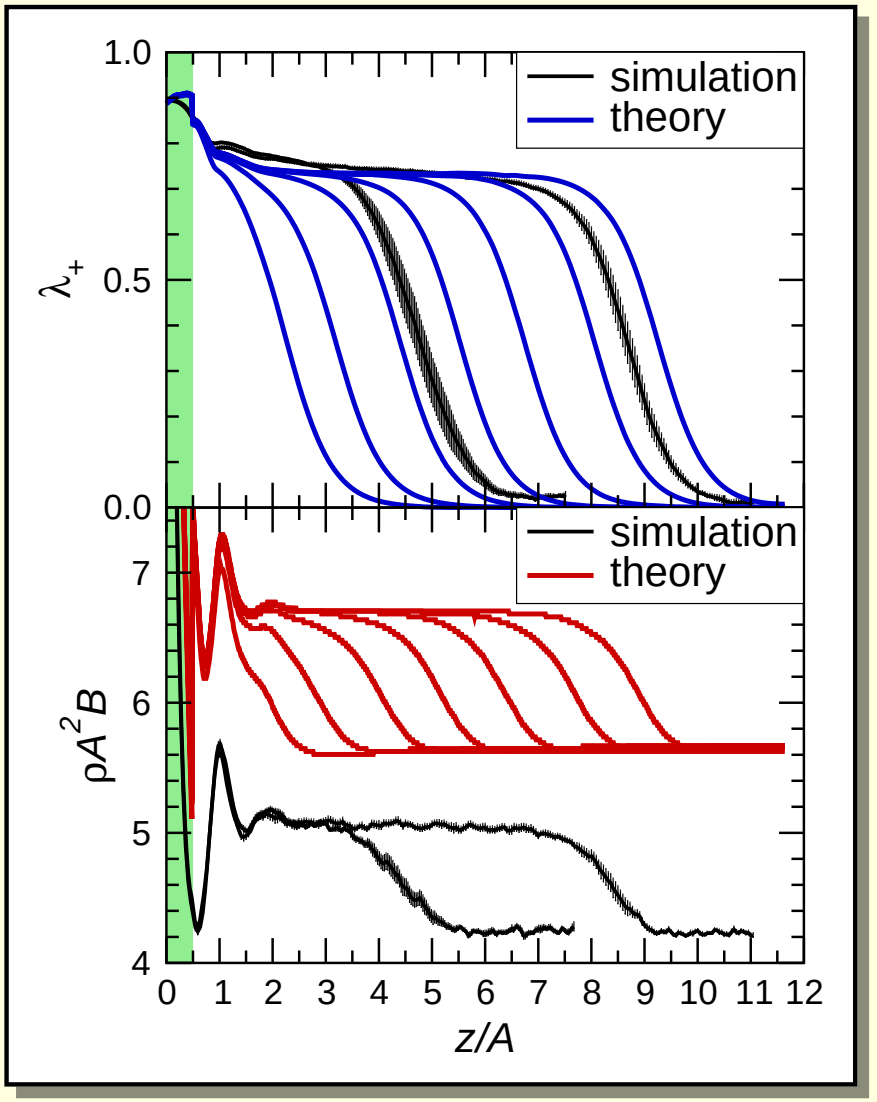

Competing boundaries

At the equilibrium I-N interface, planar alignment is favoured; at the solid wall, this may not be so.

Director rotates:

- $\theta = 0°$, normal to wall;
- $\theta = 30°, 60°$, tilted.
- $\theta = 90°$, in plane of wall.

Profiles determined by:

- anchoring W at wall;
- anchoring W at interface;
- elastic constant K_{33} in film.

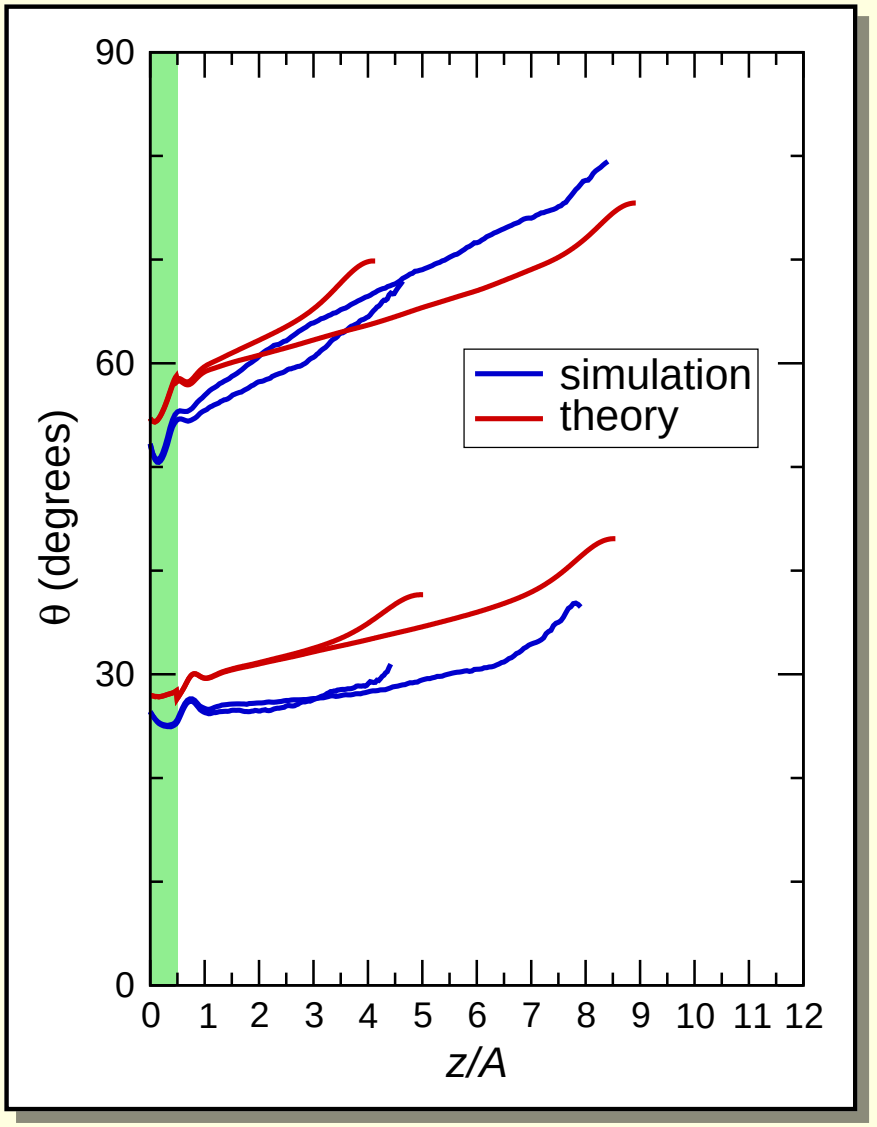

Interface snapshots

Solid surface anchoring at $\theta = 0°$ and $\theta = 90°$.

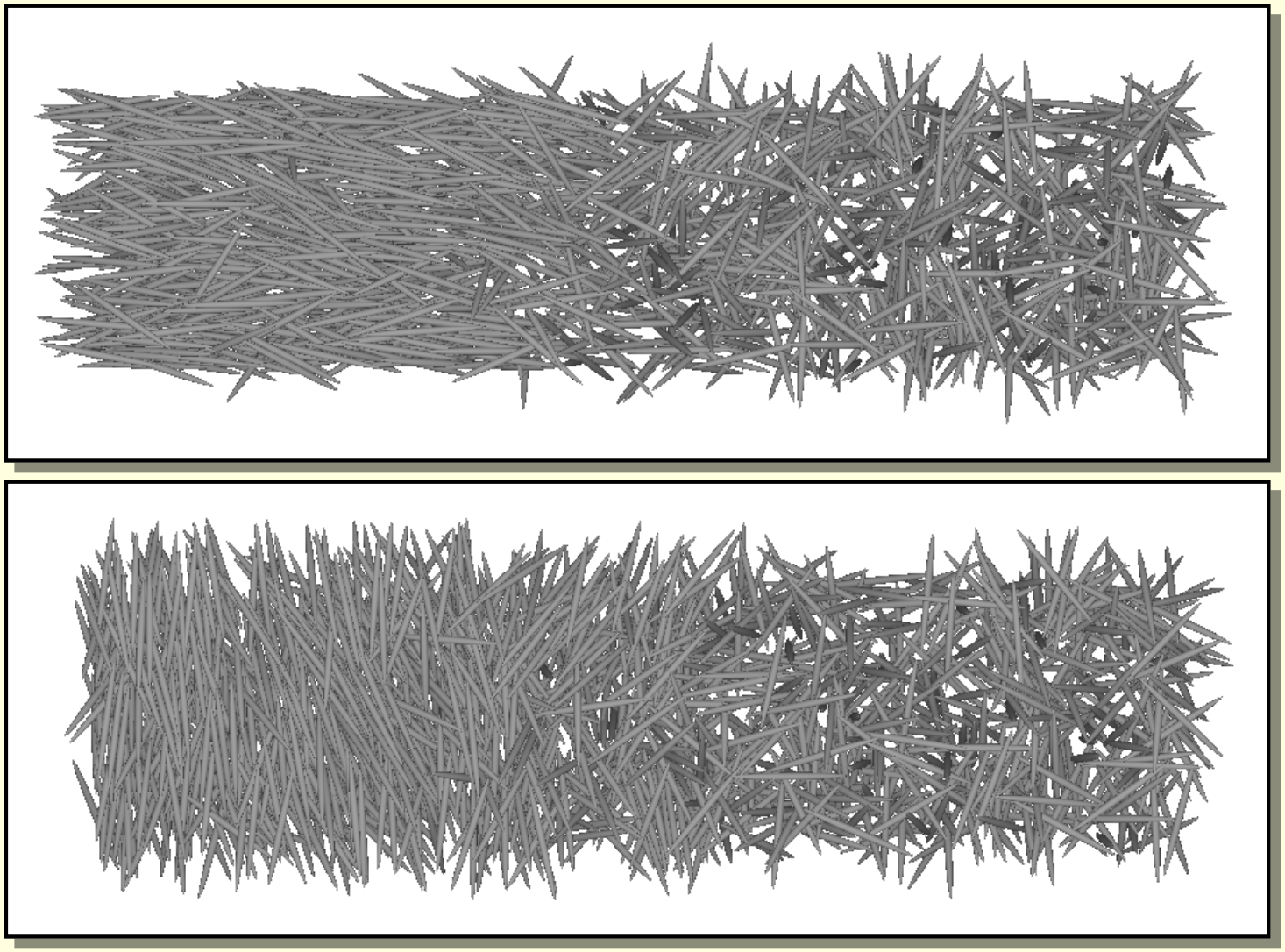

Interface snapshots

Solid surface anchoring at $\theta = 30°$ and $\theta = 60°$.

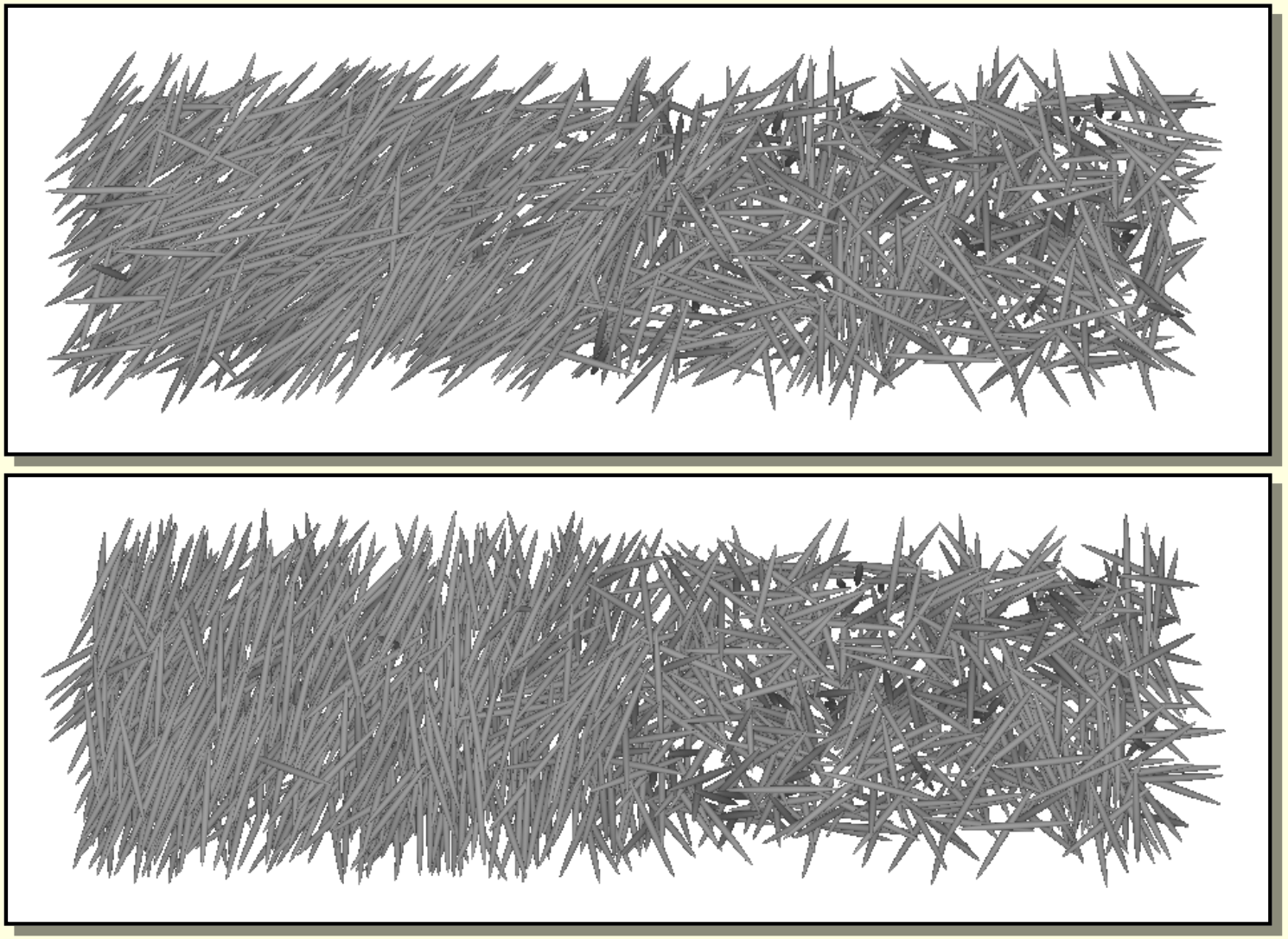

Surface Tension

For a planar interface, normal to the z-direction, a microscopic expression for surface tension γ is:

$$\gamma = \int_{-\infty}^{\infty} \mathrm{d}z \; [P_{\mathrm{N}} - P_{\mathrm{T}}(z)] \equiv \int_{-\infty}^{\infty} \mathrm{d}z \; \pi(z) \; .$$

- $P_{\mathrm{N}} = P_{zz} = P$ is the normal component of pressure tensor $\mathbf{P}$;
- P_{N} is independent of z throughout the system;
- $P_{\mathrm{T}}(z) = P_{xx}(z) = P_{yy}(z)$ is the transverse component of $\mathbf{P}$;
- P_{T} varies with z near interfaces;
- Far from the interface, $P_{\mathrm{T}}(z) = P_{\mathrm{N}} = P$.

Surface Tension Profiles

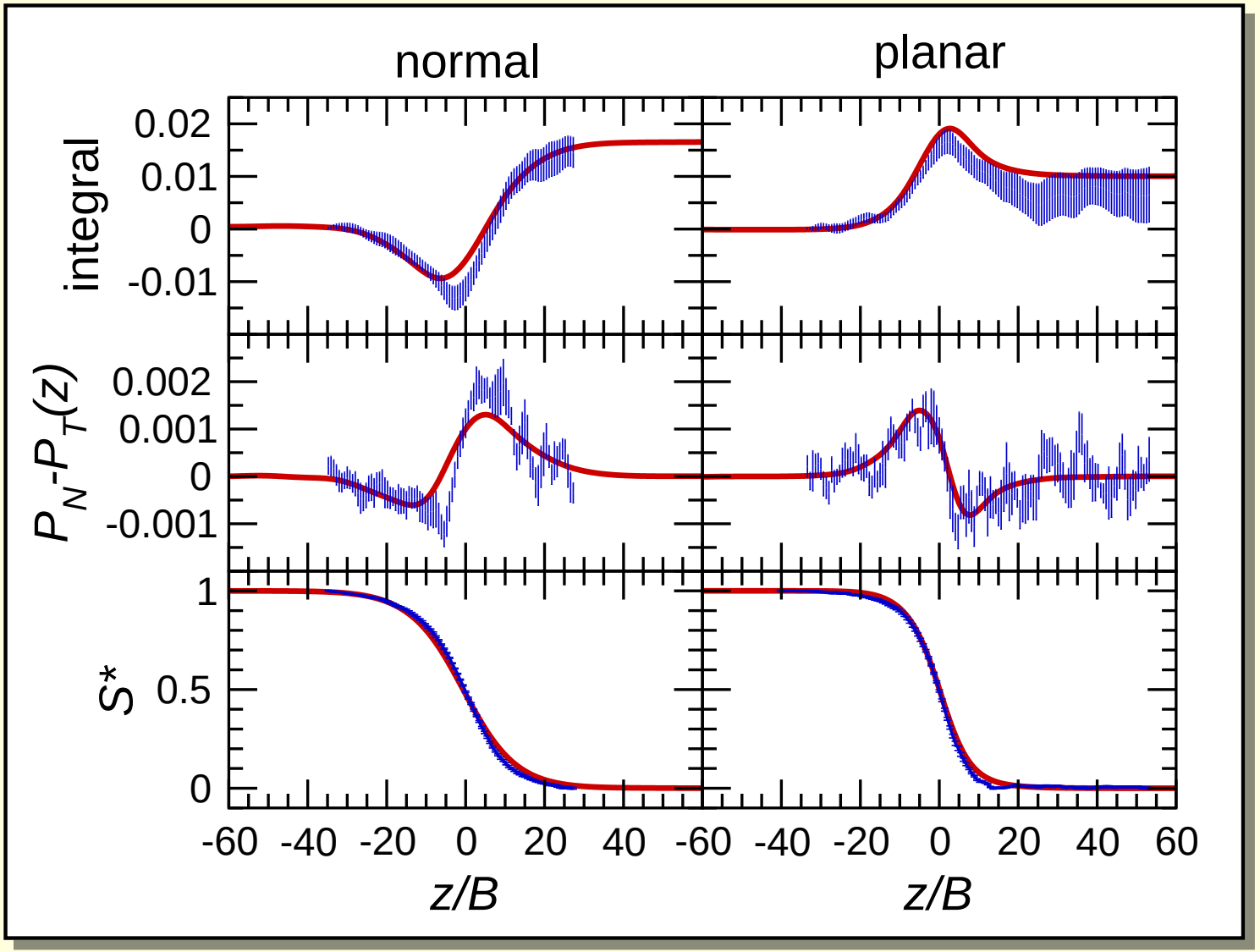

Capillary waves

The Onsager theory *neglects* capillary wave fluctuations of the interface; these are also suppressed in computer simulations with insufficient transverse box dimensions. However, they may be detected by using larger boxes and doing a block-size analysis. Considering the deviation $h(x,y) = z_{\mathrm{int}}(x,y) - \bar{z}_{\mathrm{int}}$ of the interfacial position from its averaged position, and disregarding the bending rigidity of the interface, the capillary wave Hamiltonian is given by

$$\mathcal{H}_{\mathrm{CW}} = \frac{\gamma}{2}\int \mathrm{d}x\mathrm{d}y \left[\left(\frac{\partial h}{\partial x}\right)^2 + \left(\frac{\partial h}{\partial y}\right)^2\right] = \frac{\gamma}{2}\sum_{\boldsymbol{q}} q^2 |h(\boldsymbol{q})|^2$$

where γ is the interfacial tension and the second step follows by Fourier transformation.

Simulation Results

- We studied a system of $N = 115200$ soft ellipsoids with $A/B = 15$, in a periodic box with dimensions
  - $L_x = L_y \equiv L \approx 150B = 10A$
  - $L_z \approx 300B = 20A$.
- A nematic-isotropic film system was prepared and allowed to stabilize: 1.2×10^6 MD steps were allowed for equilibration, and about 2.0×10^6 MD steps to collect data.
- In order to study the interfacial position fluctuations, we split our system into columns of block size $\ell \times \ell$, height L_z.
- Interface position $z_{\mathrm{int}}(x, y)$ in each column estimated and used to calculate interface widths and positions as a function of ℓ.

Interface position distribution

From $\mathcal{H}_{\rm CW}$, and equipartition,

$$\langle |h(\boldsymbol{q})|^2 \rangle = k_{\rm B}T/\gamma q^2$$

so local interface position fluctuations should be Gaussian

$$P(h) = (2\pi s^2)^{-1/2} \exp(-h^2/2s^2)$$

$$s^2 = \langle h^2(x,y) \rangle$$

$$= \frac{1}{4\pi^2} \int \mathrm{d}\boldsymbol{q} \langle |h(\boldsymbol{q})|^2 \rangle$$

$$= (k_{\rm B}T/2\pi\gamma) \ln (q_{\rm max}/q_{\rm min})$$

$q_{\rm max} \sim 2\pi/\ell$, $q_{\rm min} \sim 2\pi/L$.

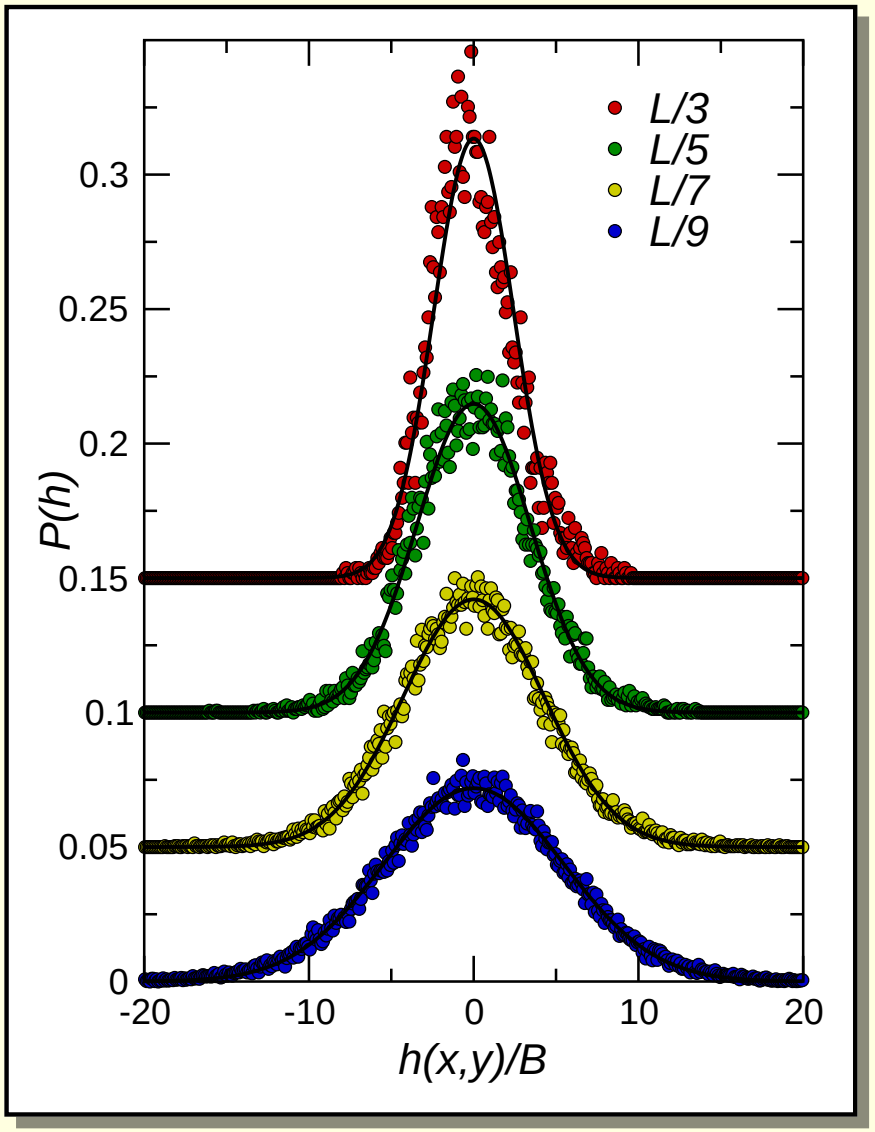

Interface width

Squared interfacial width, W^2 also depends on block size ℓ:

$$W^2 = W_0^2 + (\pi/2)s^2$$

$$= W_0^2 + (k_B T/4\gamma) \ln\left(\frac{q_{max}}{q_{min}}\right)$$

$q_{max} \sim 2\pi/A$, $q_{min} \sim 2\pi/\ell$.

- Our results are consistent with capillary wave theory
- This gives an estimate of $\gamma AB/k_B T \sim 0.24$.

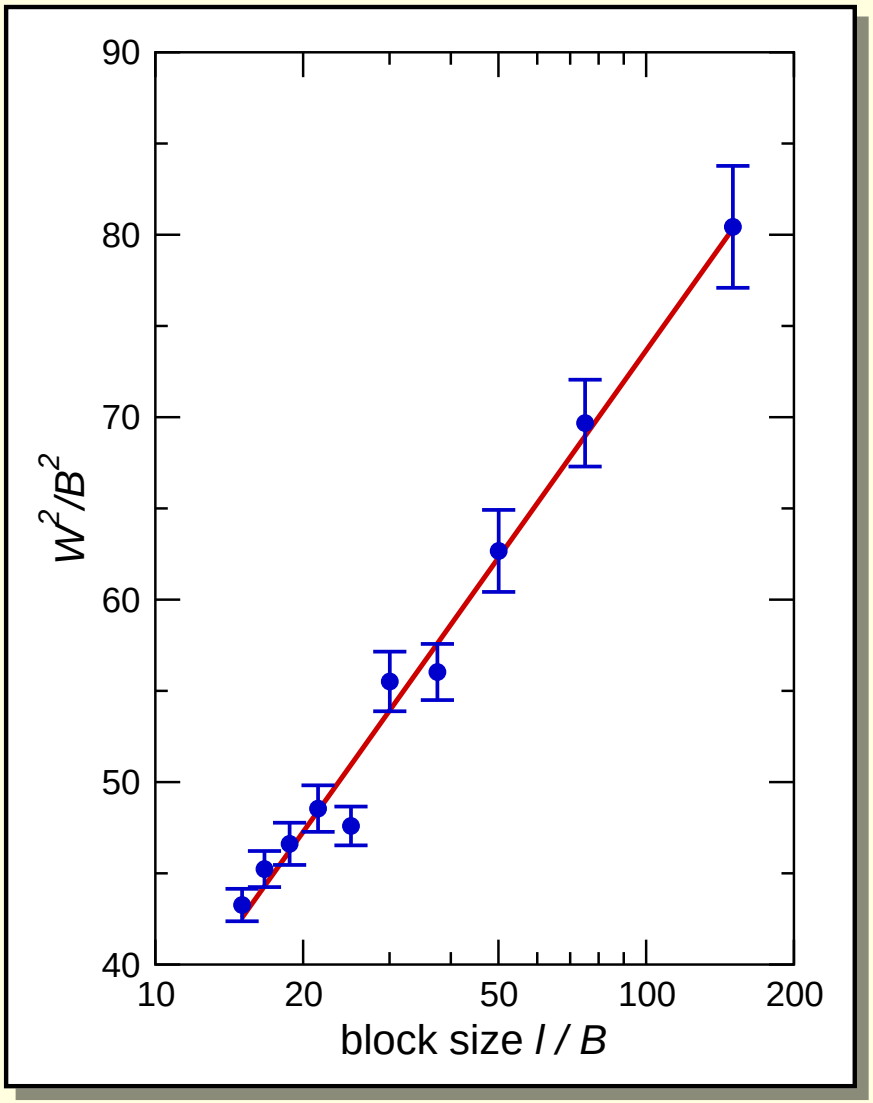

Anisotropy of Capillary Waves

- We also study the difference in the capillary wave spectrum parallel and normal to the director.
- Typical results are shown in the figure for $\ell = L/8$.

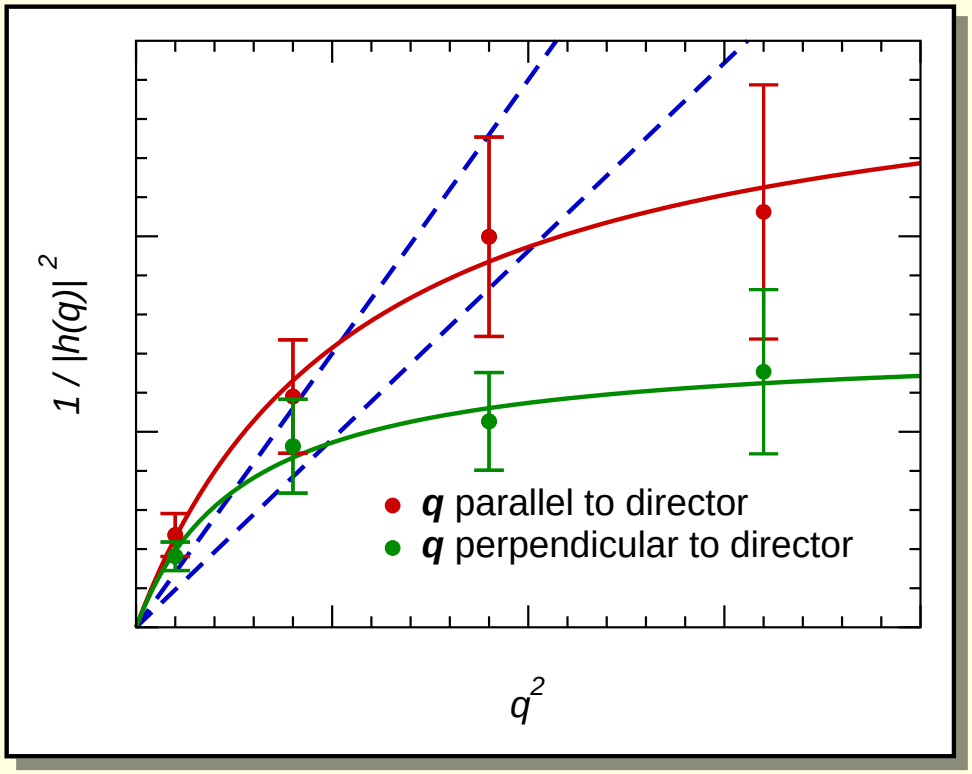

The low-q behaviour is consistent with the value of γ deduced from the interface width. From the figure it seems that the capillary wave spectrum is anisotropic at higher values of q.

Colloidal Suspensions

Macroparticles (solid or liquid) introduced into liquid crystals considerably influence their electro-optical properties. Experiments.

- A macroparticle distorts the director distribution;
- effective long-range interaction between macroparticles;
- new supermolecular structures, e.g. threadlike structures consisting of macroparticles.

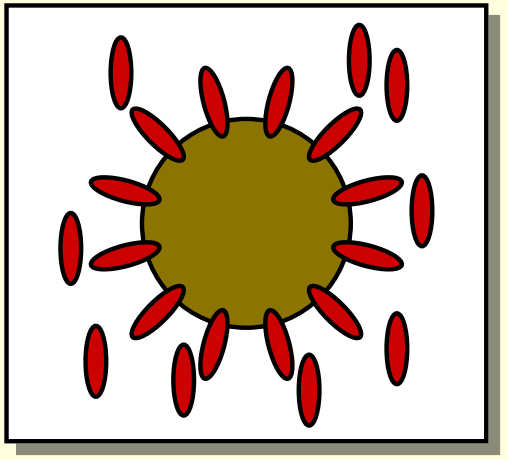

For *homeotropic* boundaries, topological mismatch between local director on surface and uniform director at large distances creates a hedgehog director configuration around particle.

Director Structures

Phenomenological theories predict two defect structures. We show director field streamlines around a spherical macroparticle.

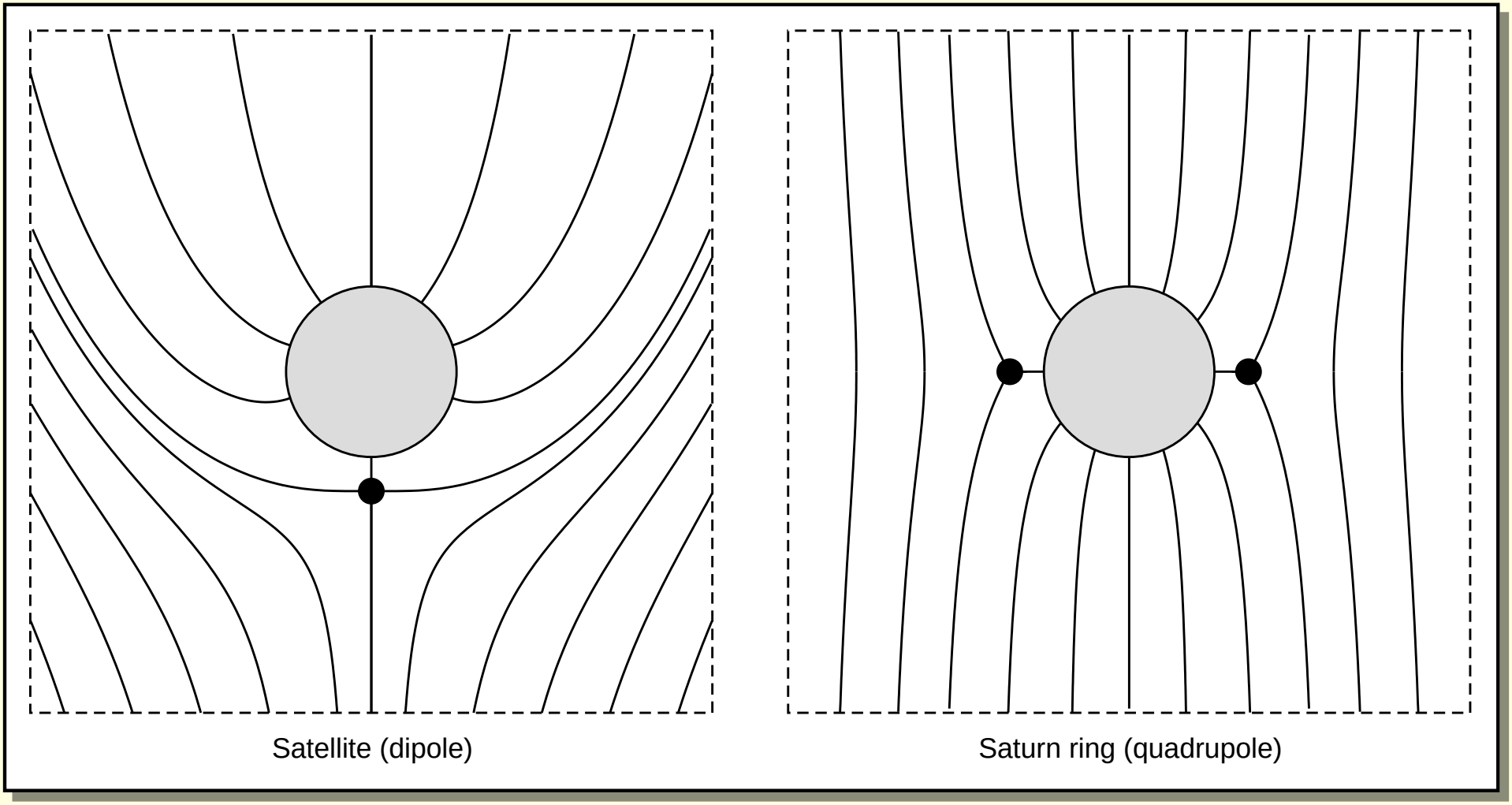

Molecular Dynamics Simulations

- $N = 64,000$–$1,000,000$
- Ellipsoidal molecules
  - Width $B = 1$
  - Length $A = 3$
  - Nematic liquid crystal phase
- Spherical Macroparticle
  - Diameter $D = 6 \ldots 30$
- Homeotropic (normal) anchoring
- Parallel MD algorithm

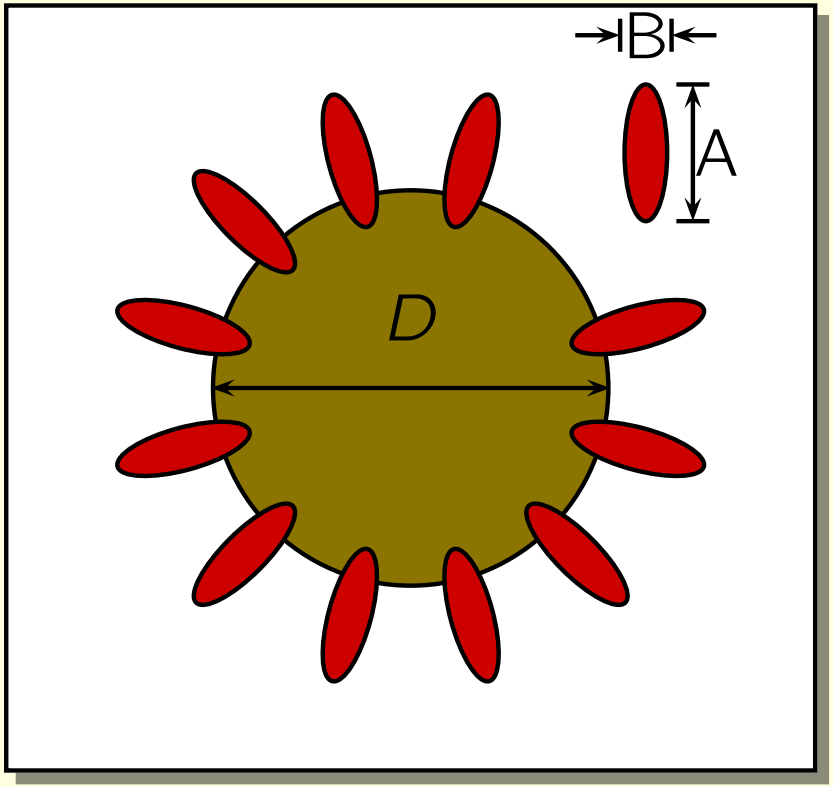

Ring defect: snapshot

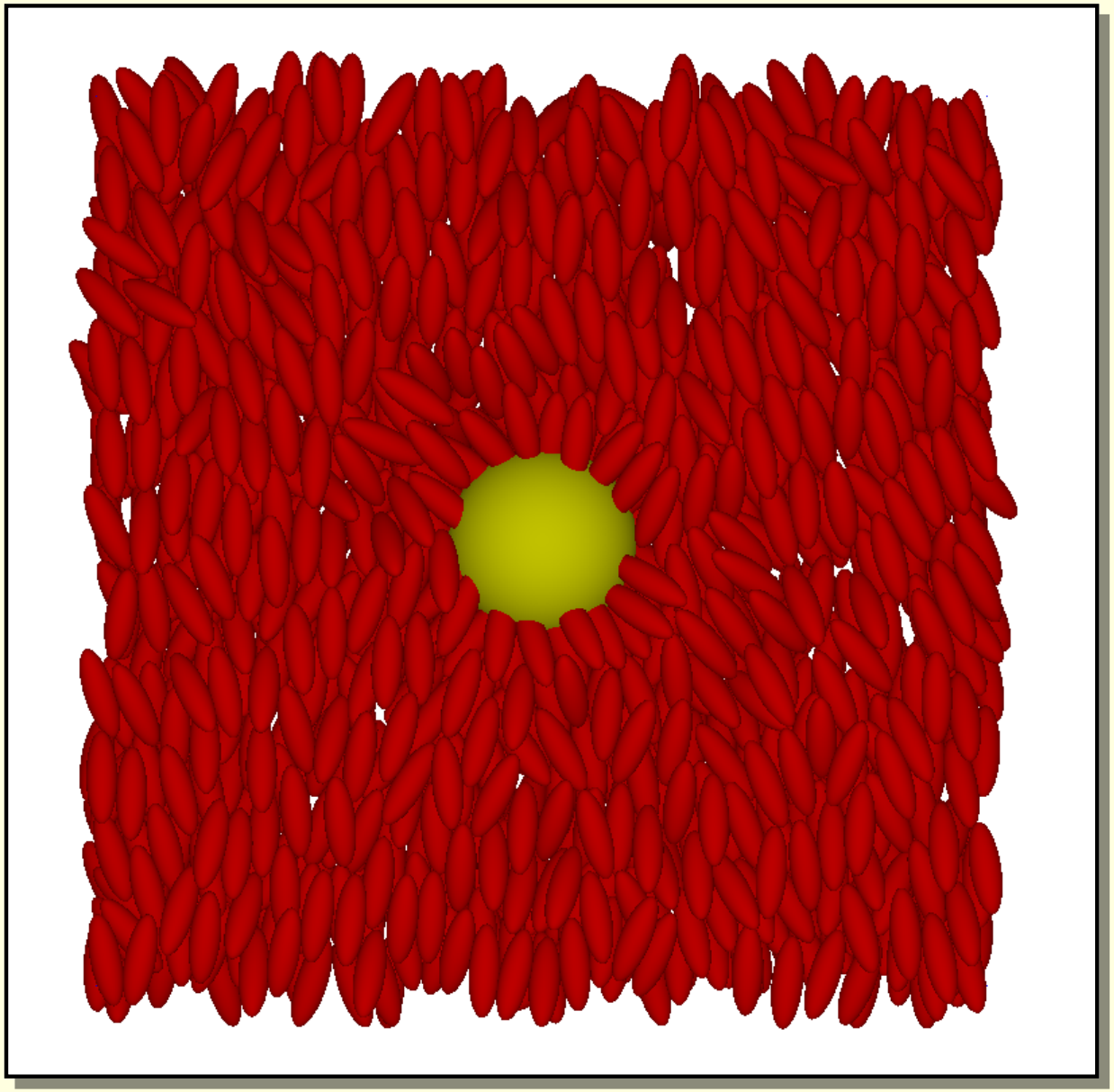

Ring defect: density

Ring defect stable for $D \leq 20$. We show slices through density map ρ:

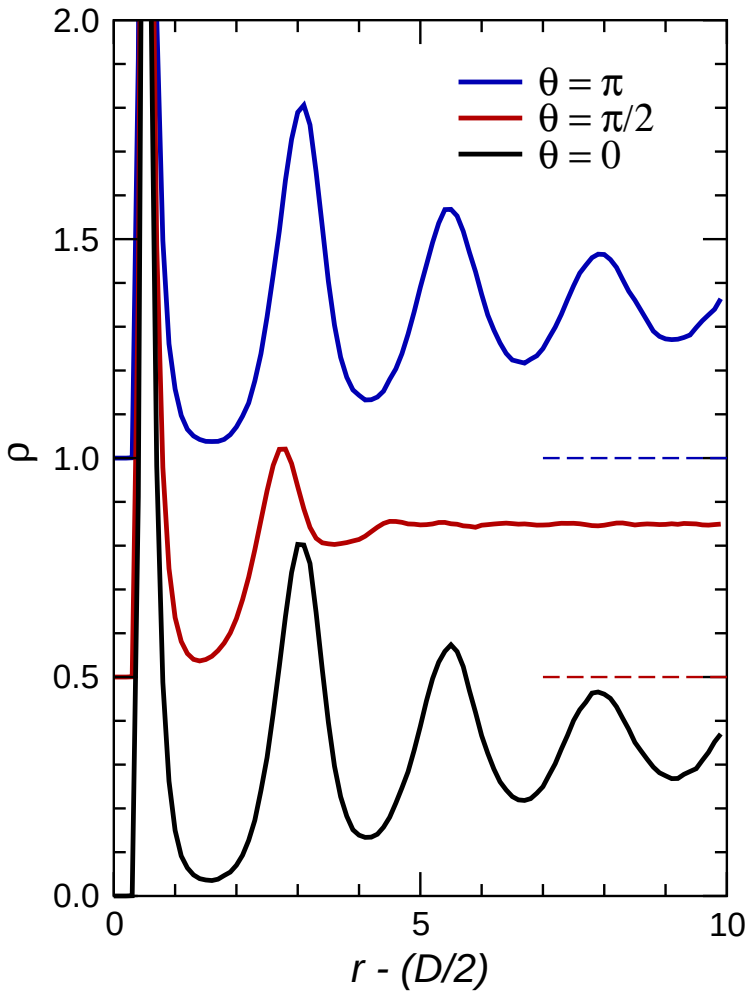

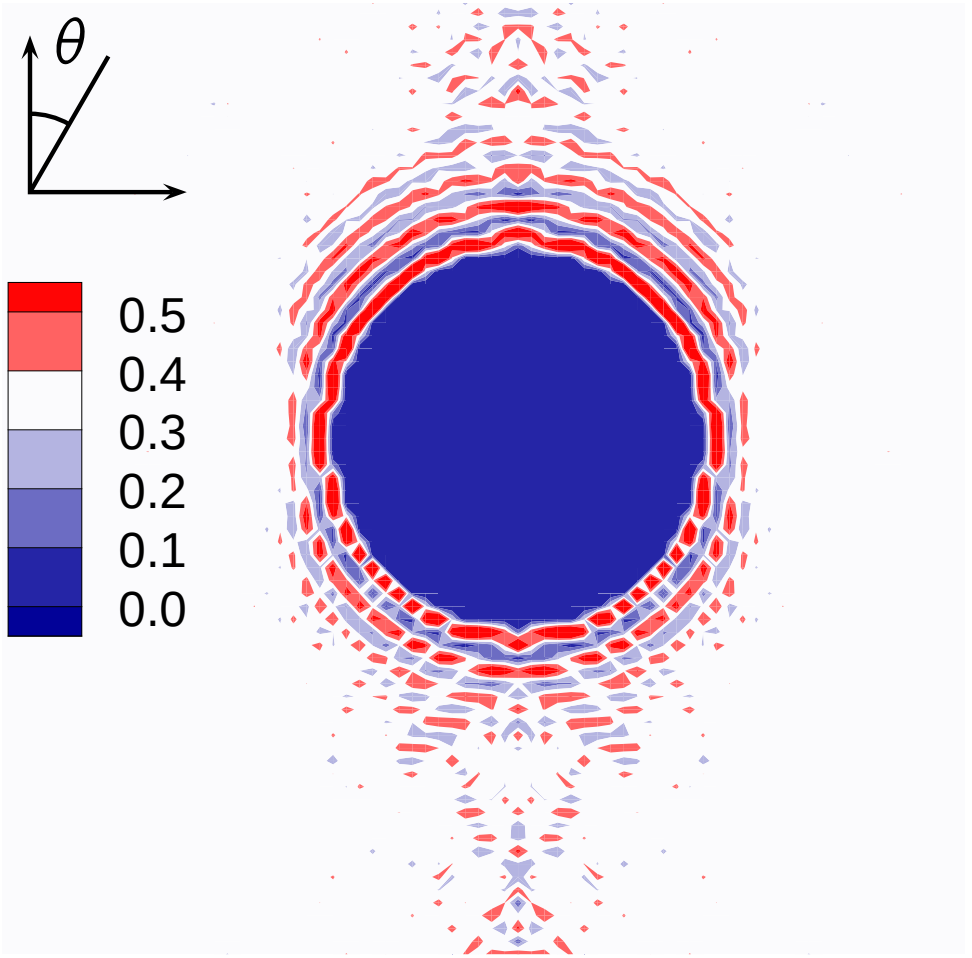

Ring defect: order

We measure orientational order S, for various particle diameters D. Here are slices in the $\theta = \pi$ direction. The disclination ring position is given by the minimum in S. More structure appears as D increases.

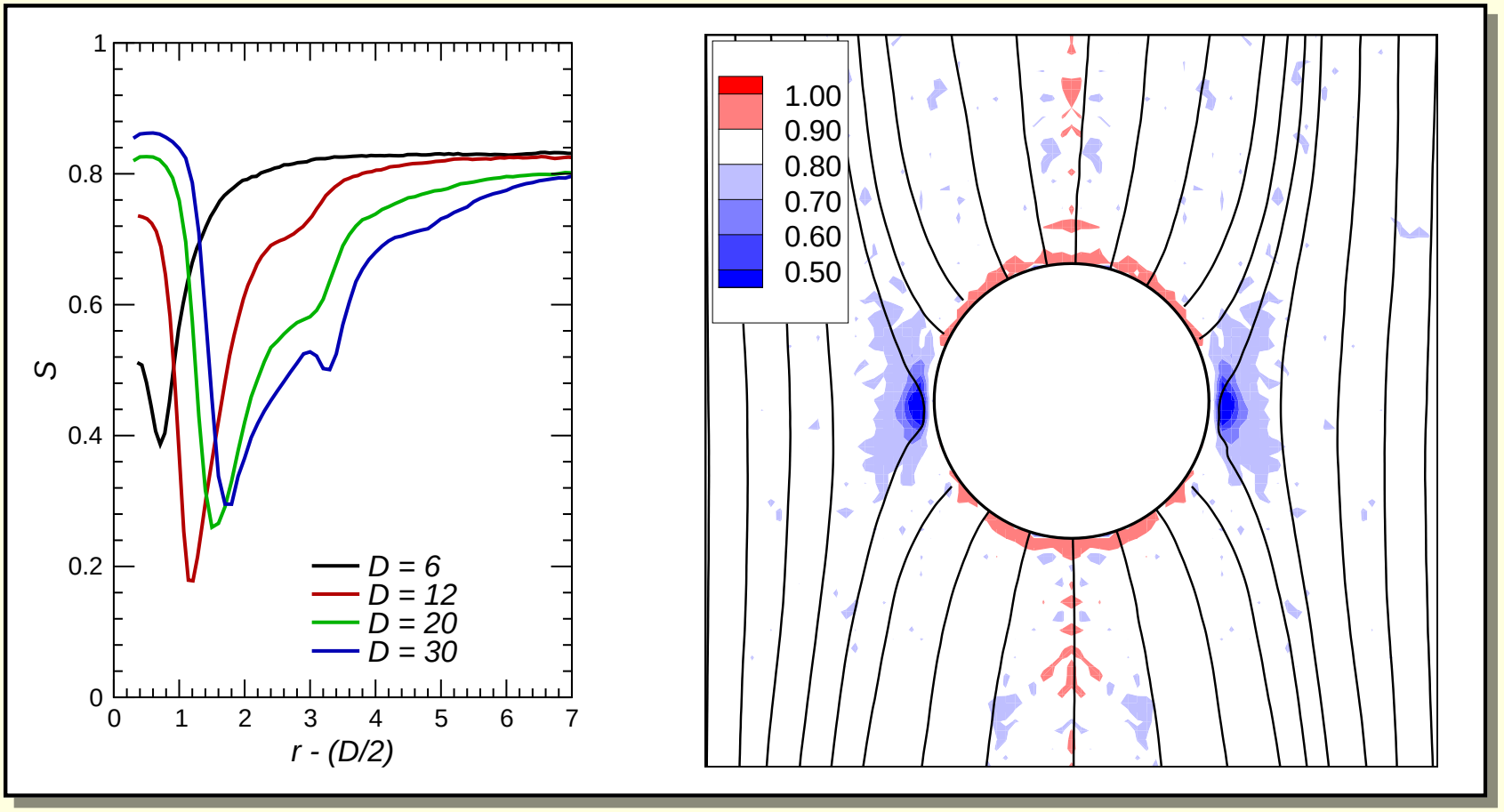

Ring size

Phenomenological theory:

$$r_{\mathrm{ring}} \approx 0.6D$$

Simulation results:

$$r_{\mathrm{ring}} = -0.33 + 0.582D.$$

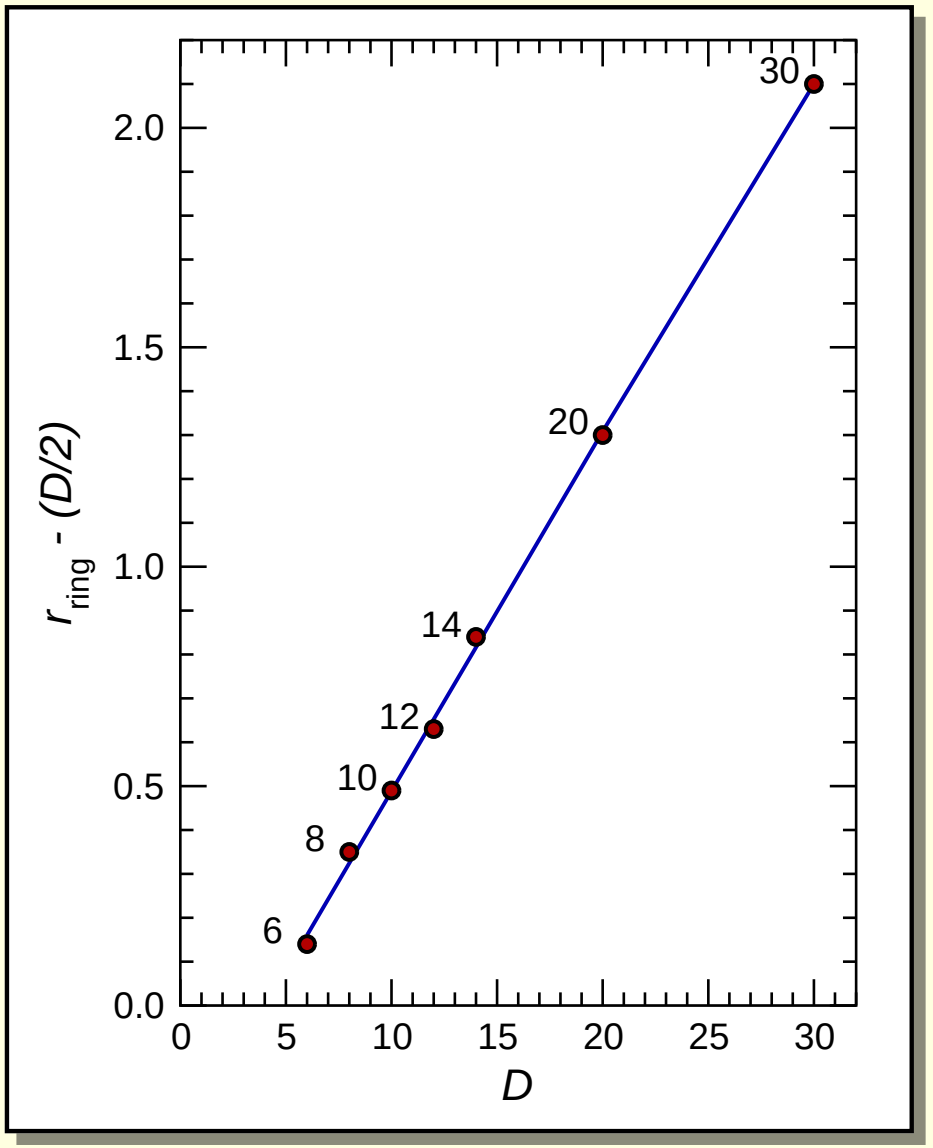

Satellite defect: snapshot

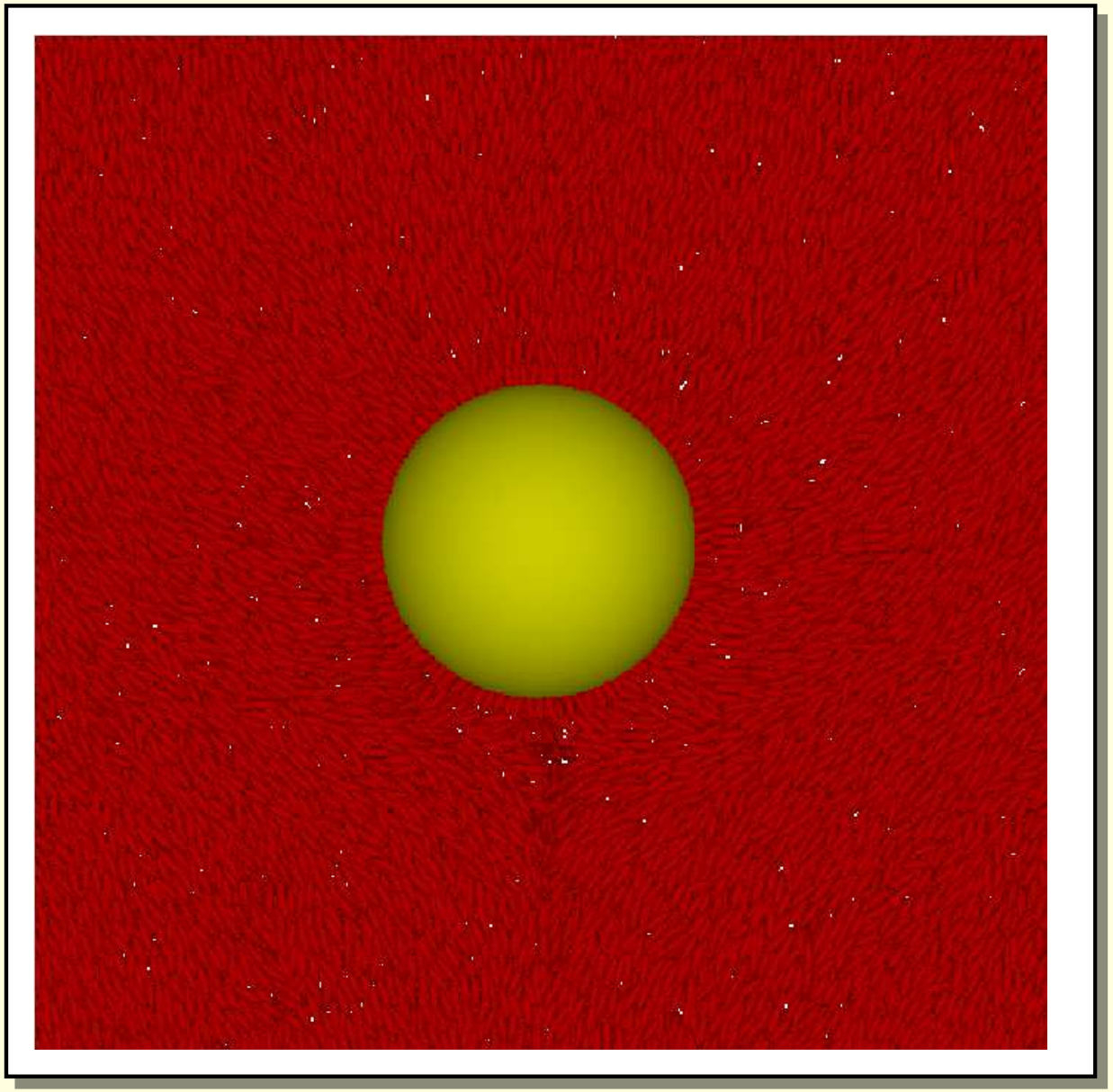

Satellite defect: density

Satellite defect stable for $D = 30$. Slices through density map:

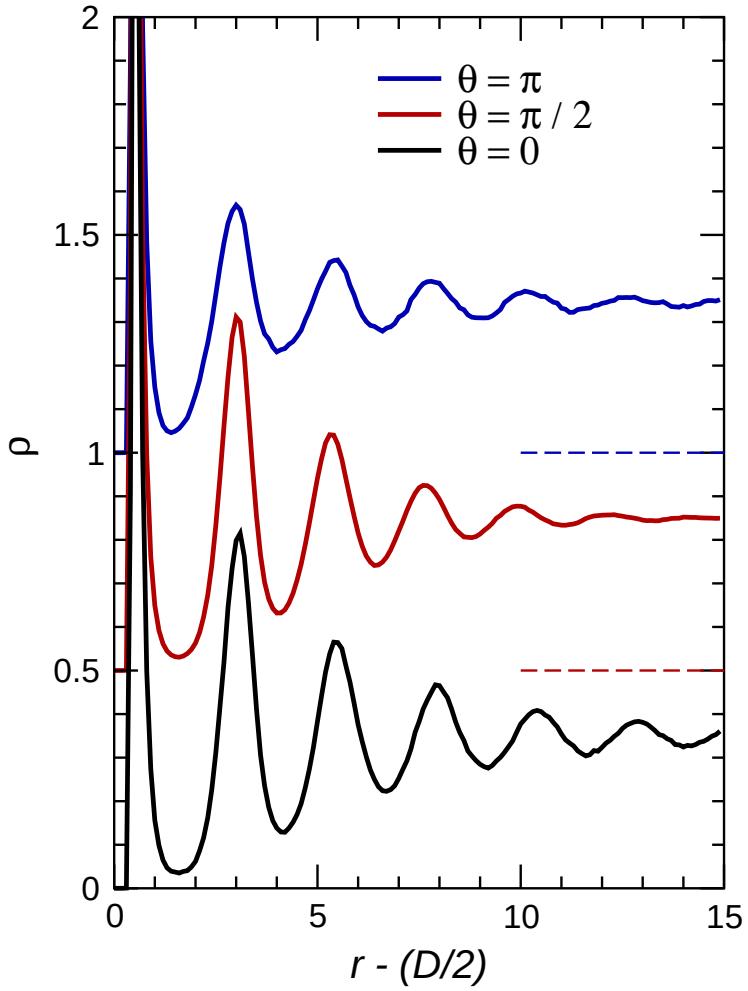

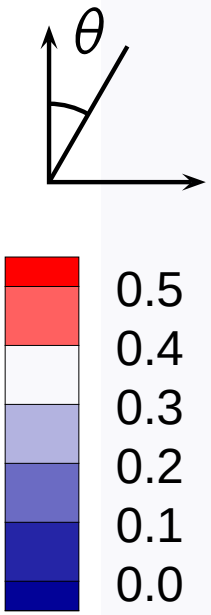

Satellite defect: order

- Centre of defect core is located at $r_{\mathrm{sat}} \approx 0.7D$.
- Theory predicts $r_{\mathrm{sat}} \approx 0.6D$.
- Highly structured defect region (not a point defect!)

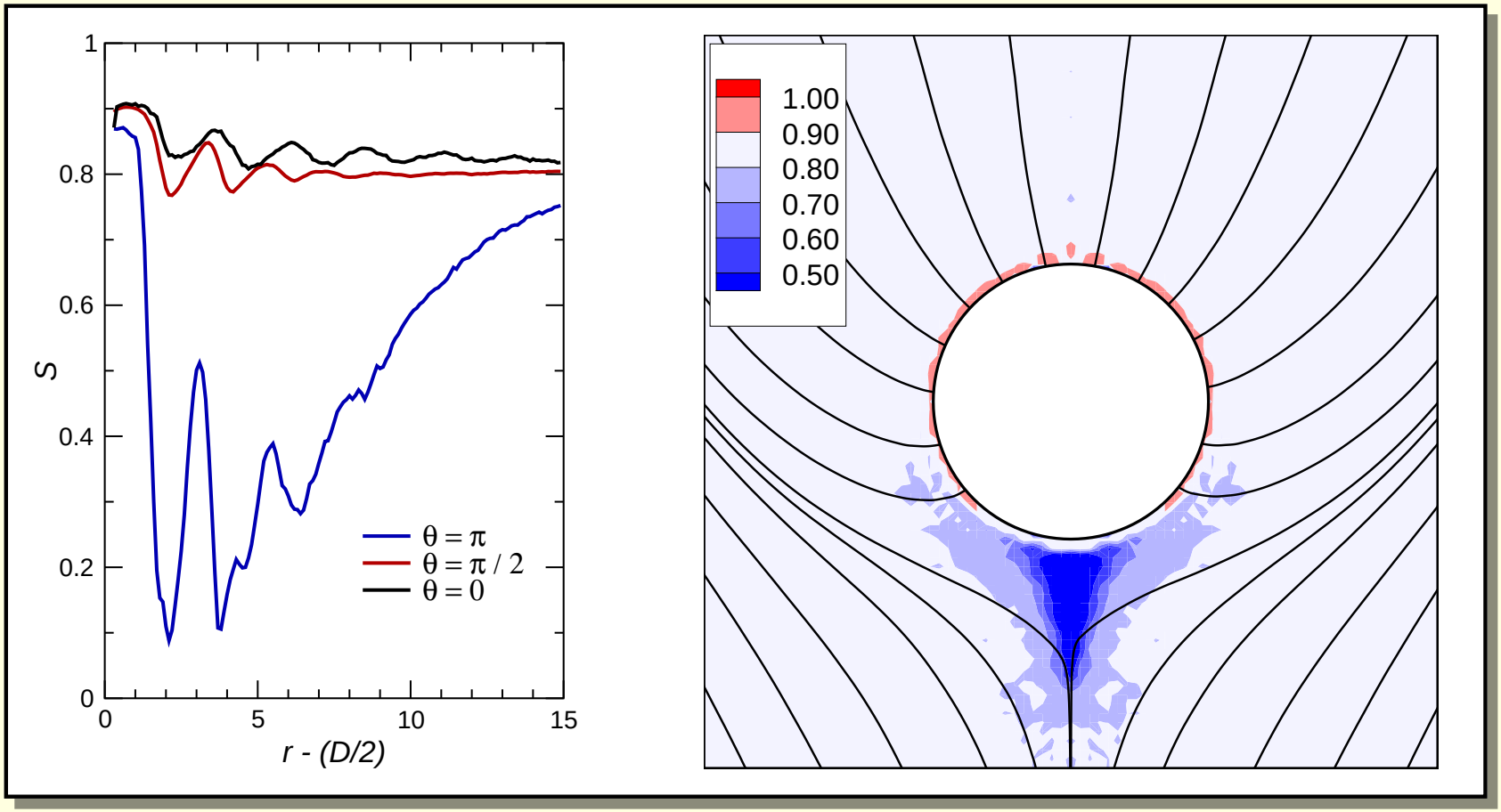

Satellite to ring conversion

- For $D = 20$ satellite evolves spontaneously into ring.
- We follow the off-centre ring position with time.

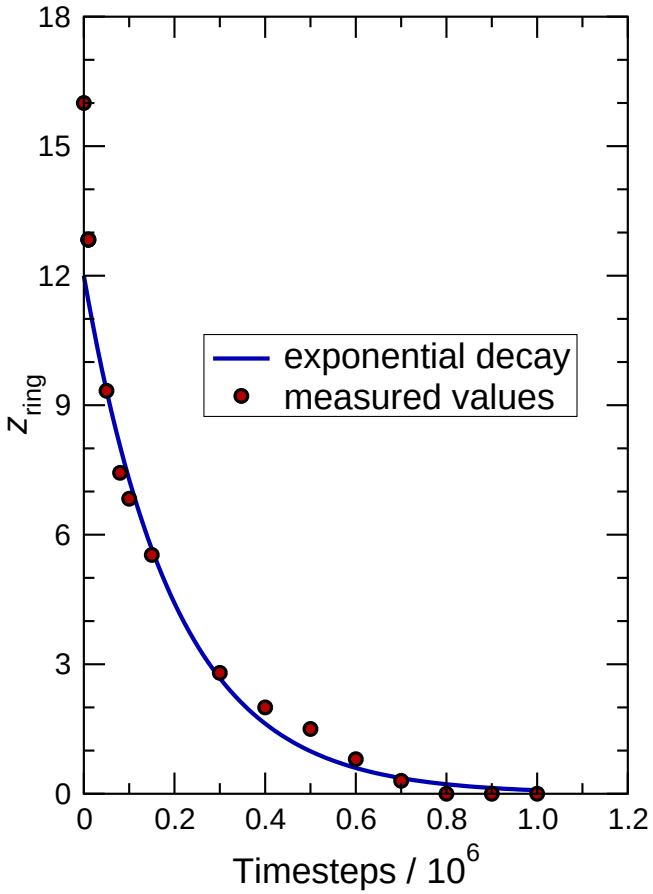

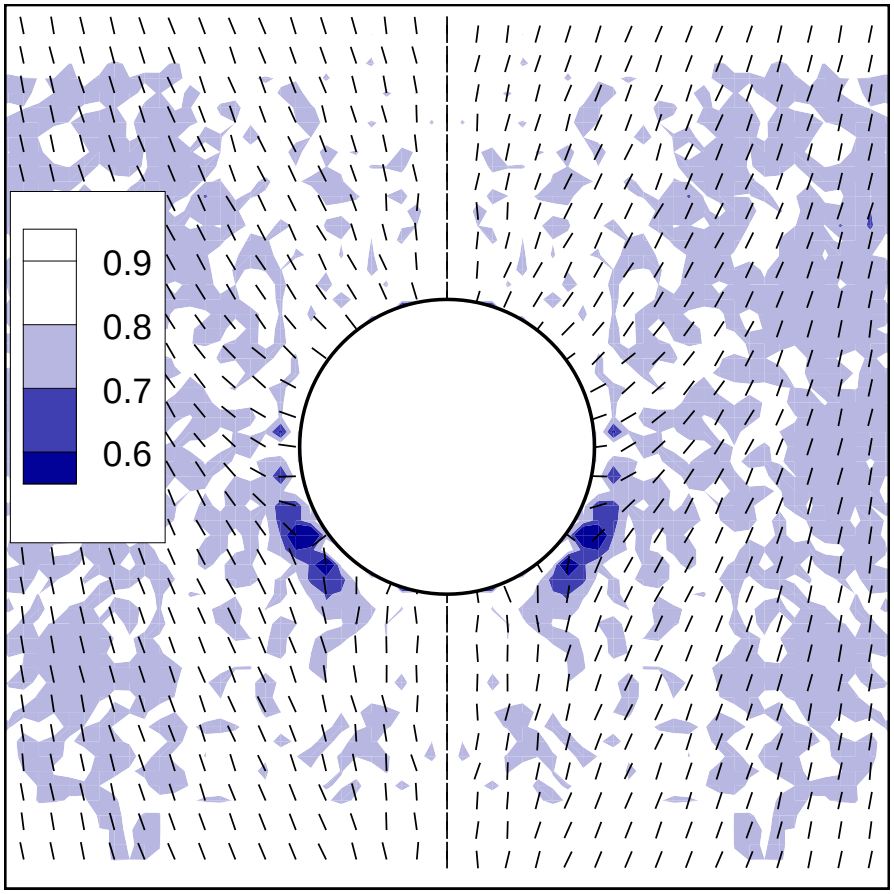

Two Macroparticles

- Ellipsoidal molecules A, B.
  - Width $B = 1$
  - Length $A = 3$
- Spherical macroparticles
  - Diameter $D = 6$
  - Separation $R = 9 \ldots 15$
- Observe distortion of director field
- Measure effective force between particles

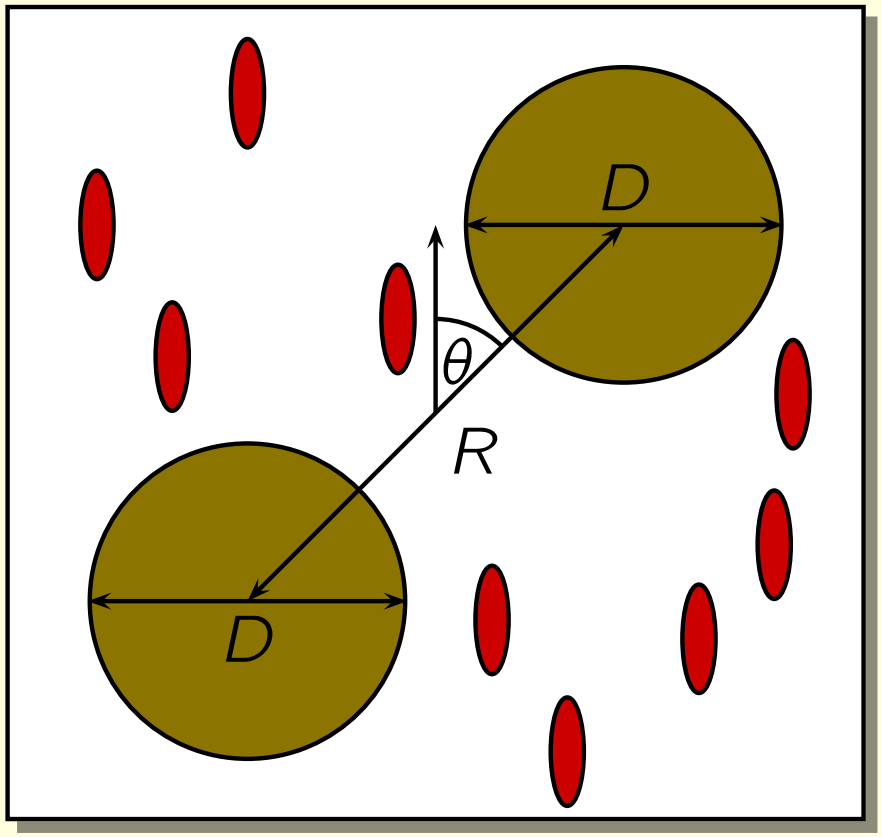

Order Map: $R = 9.0$

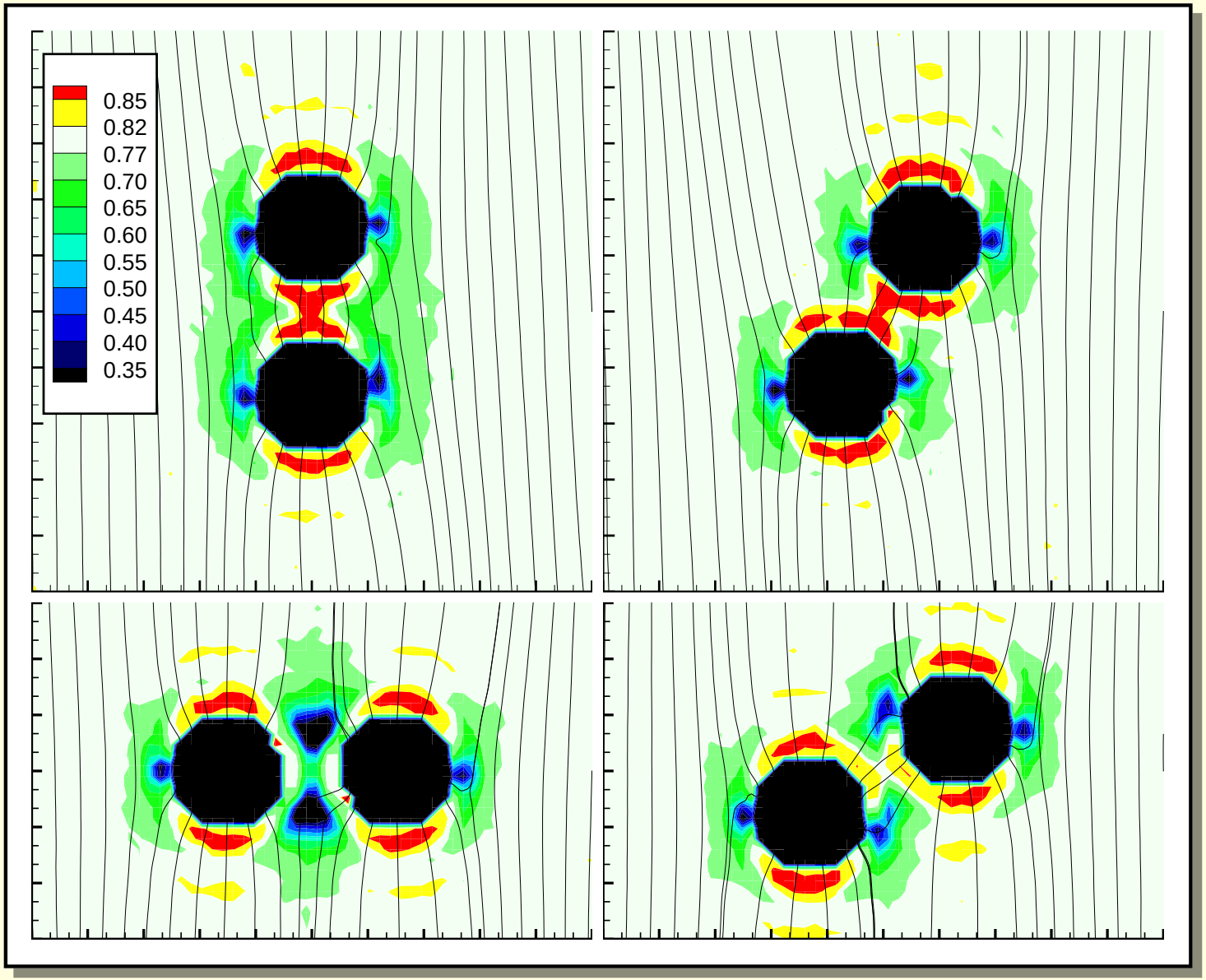

Order Map: $R = 9.5$

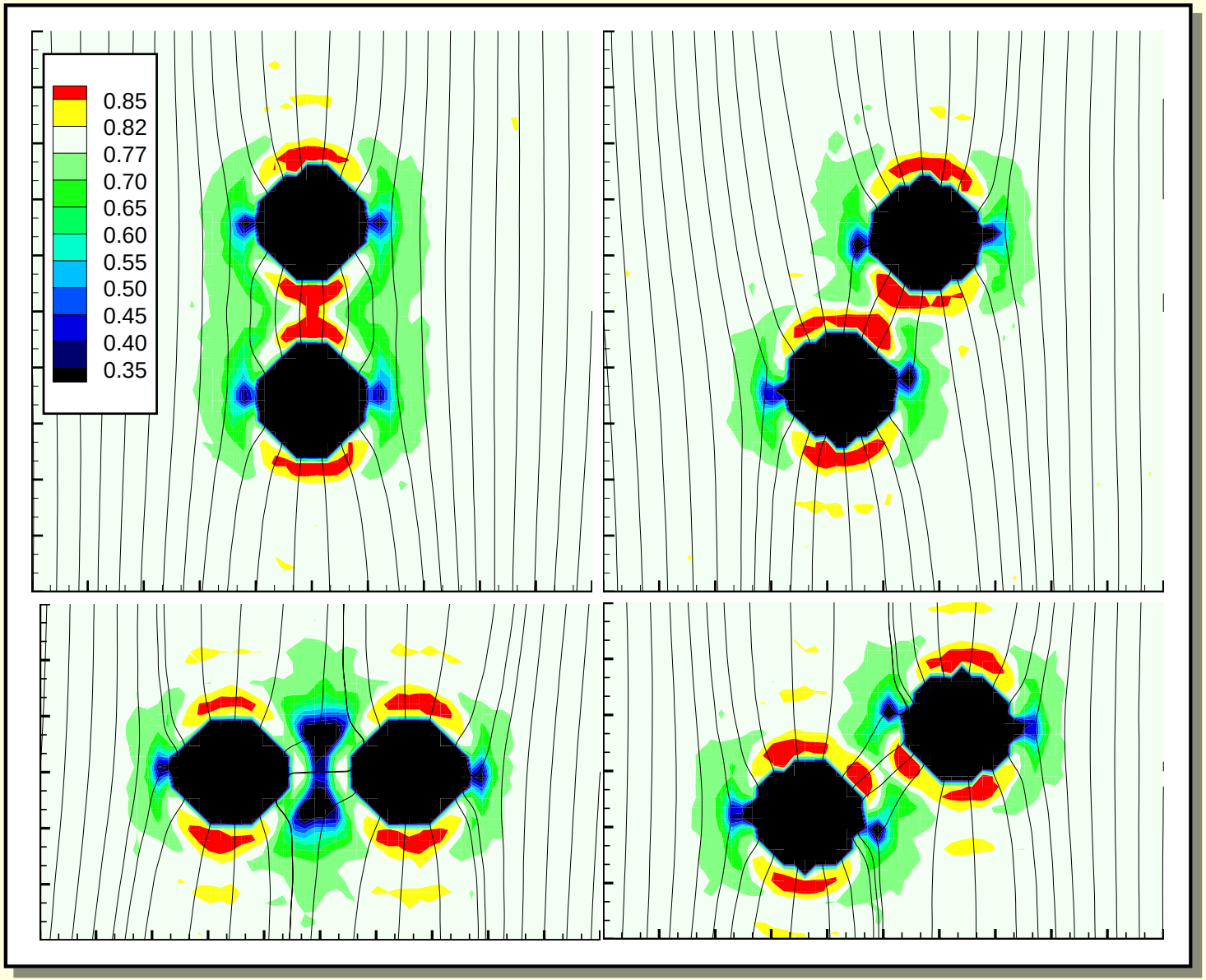

Order Map: $R = 10.0$

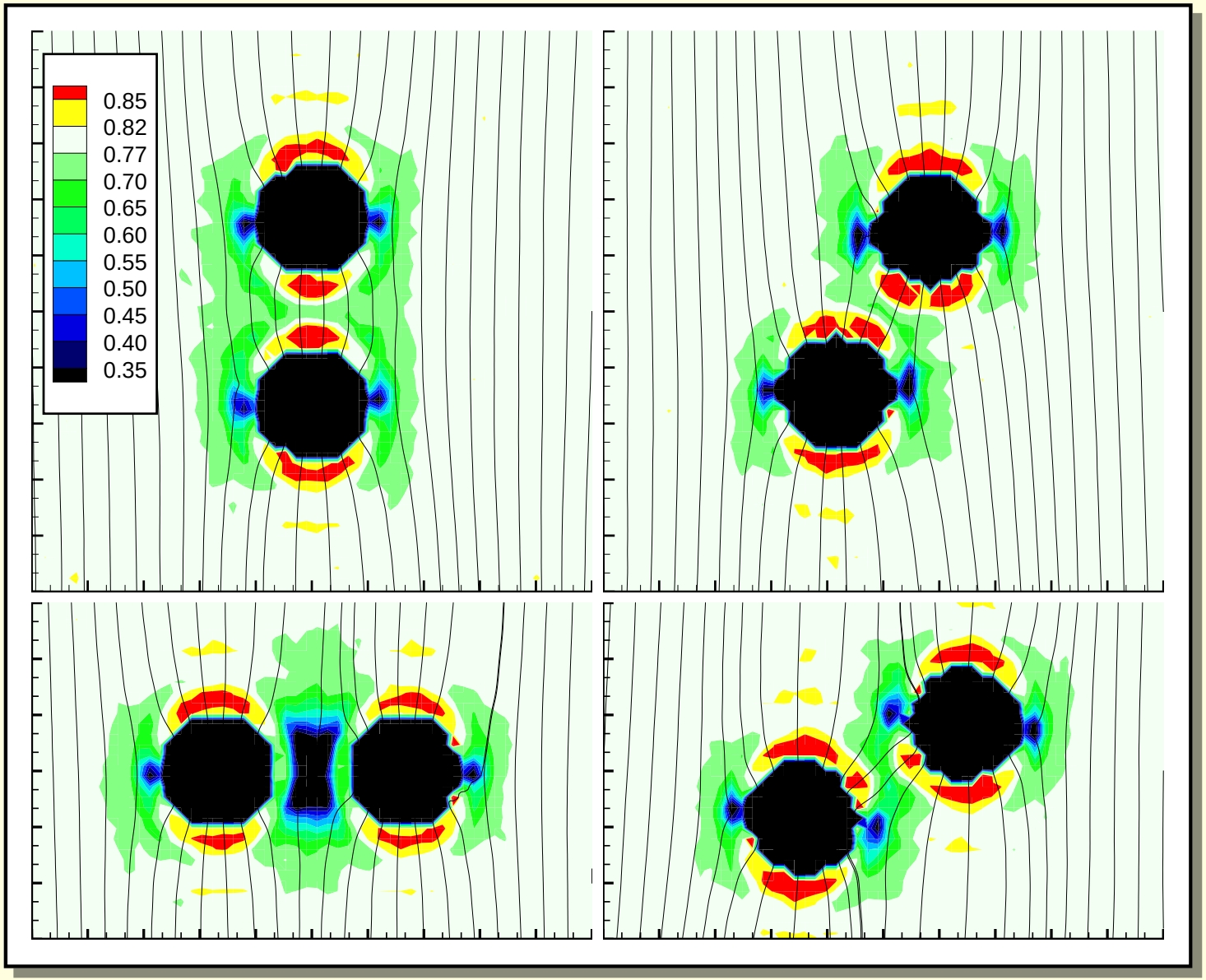

Order Map: $R = 10.5$

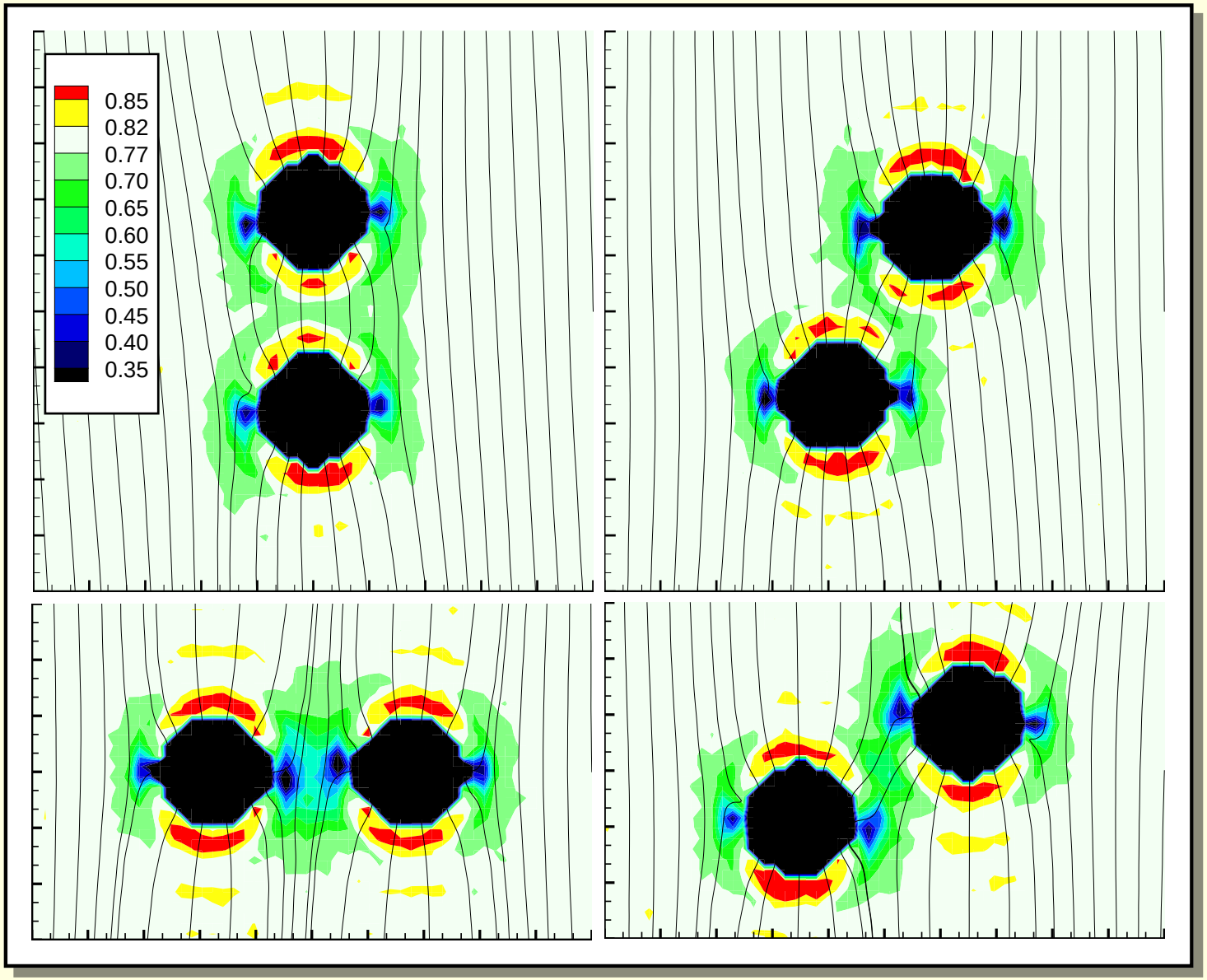

Order Map: $R = 11.0$

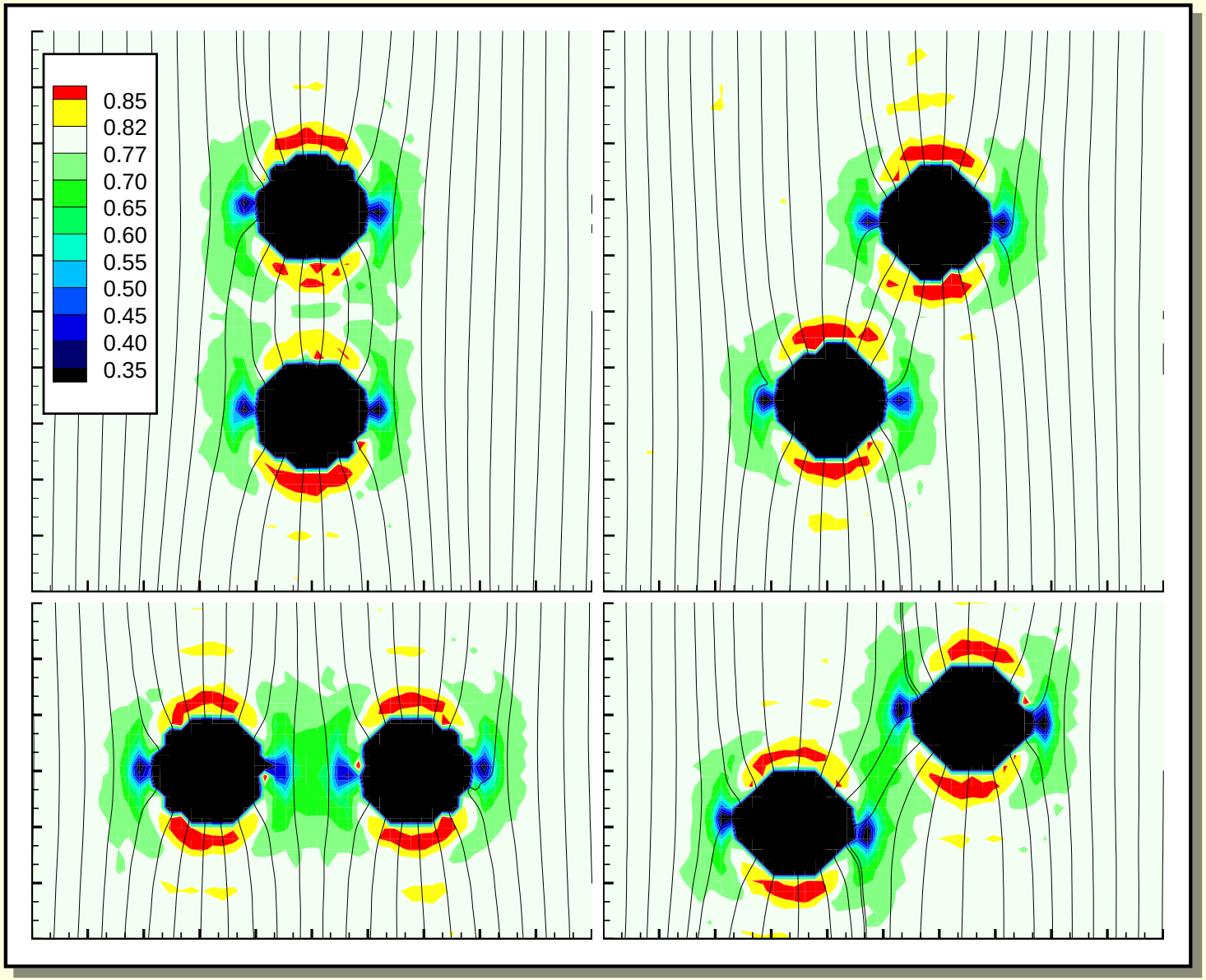

Order Map: $R = 11.5$

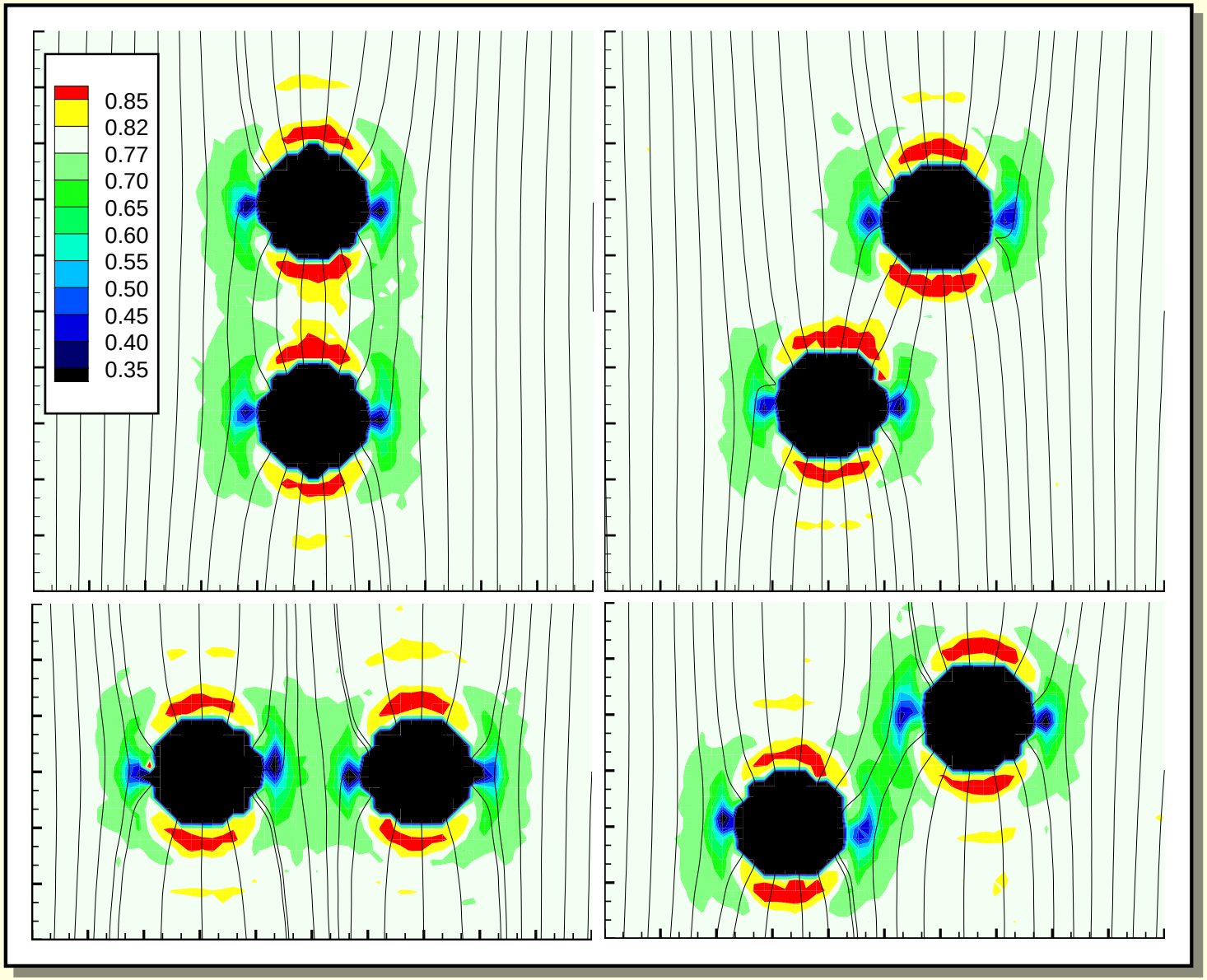

Order Map: $R = 12.0$

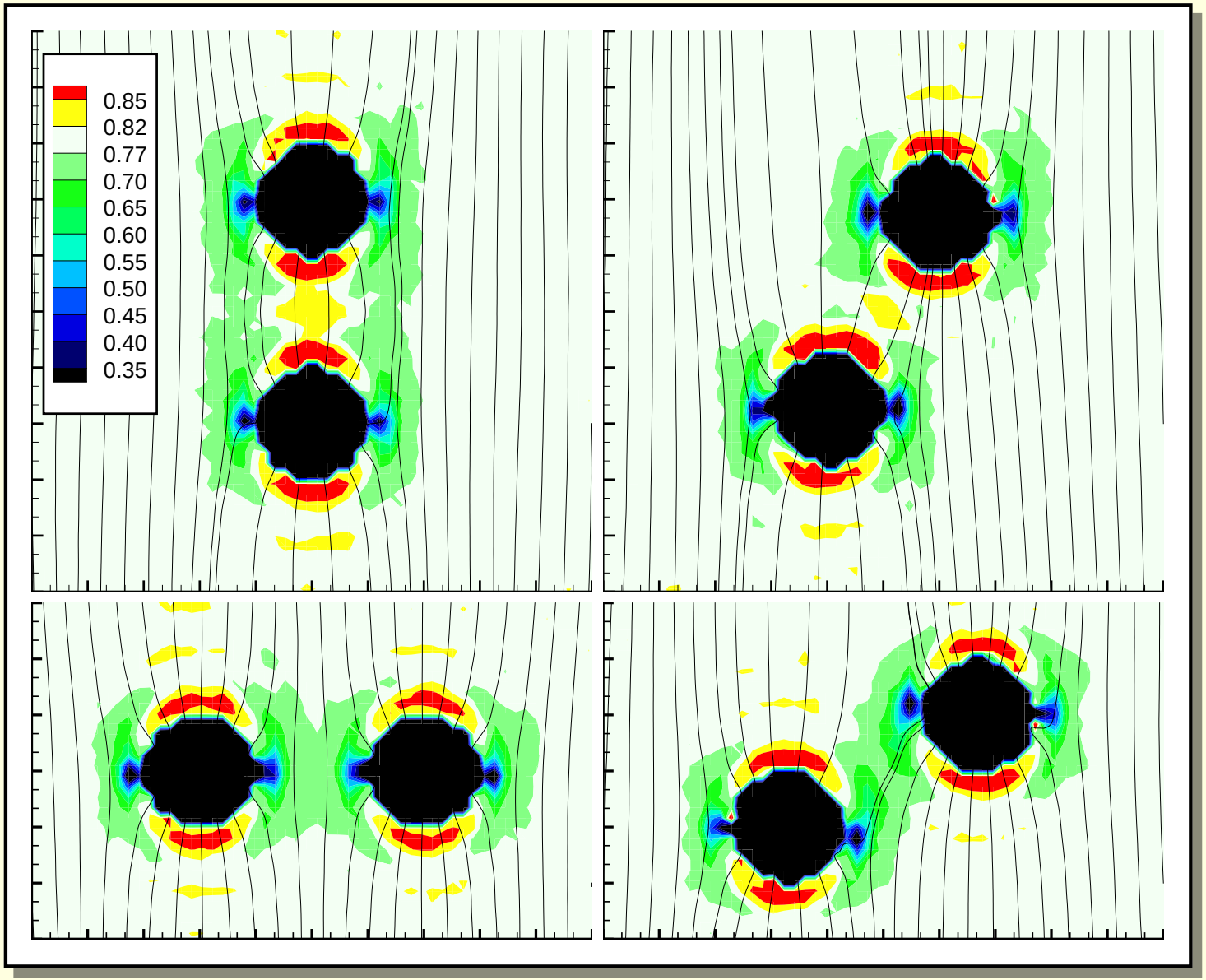

Order Map: $R = 15.0$

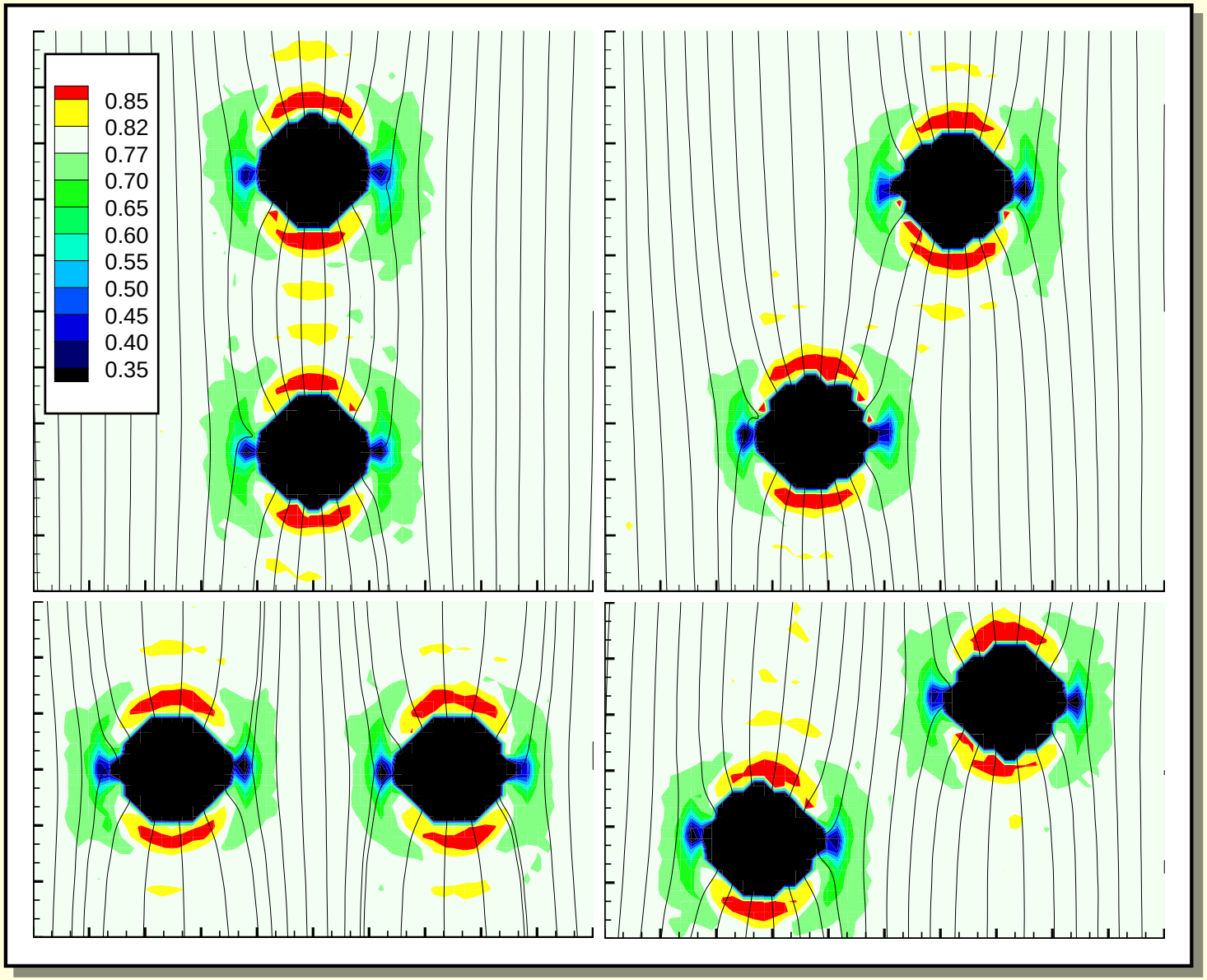

Elastic Interaction Potential

Theoretical prediction based on elastic theory:

$$\mathcal{U} \propto R^{-5}\left[9 - 20\cos 2\psi + 35\cos 4\psi\right]$$

where $\psi = \pi/2 - \theta$.

- Valid asymptotically as $R \to \infty$
- Proportionality constant depends on elastic constants
- Angular dependence is independent of elastic constants
- potential has minima with respect to angular variation at $\psi = \frac{1}{2}\arctan(4\sqrt{3}) \approx \pm 41°$, that is at $\theta \approx 49°, 131°$.

Radial Force

- Component of force along radial direction
  - ↪ line of centres
- Dominated by solvent molecule packing
- Highly structured for $\theta \neq 90^\circ$
- Structure melted for $\theta = 90^\circ$

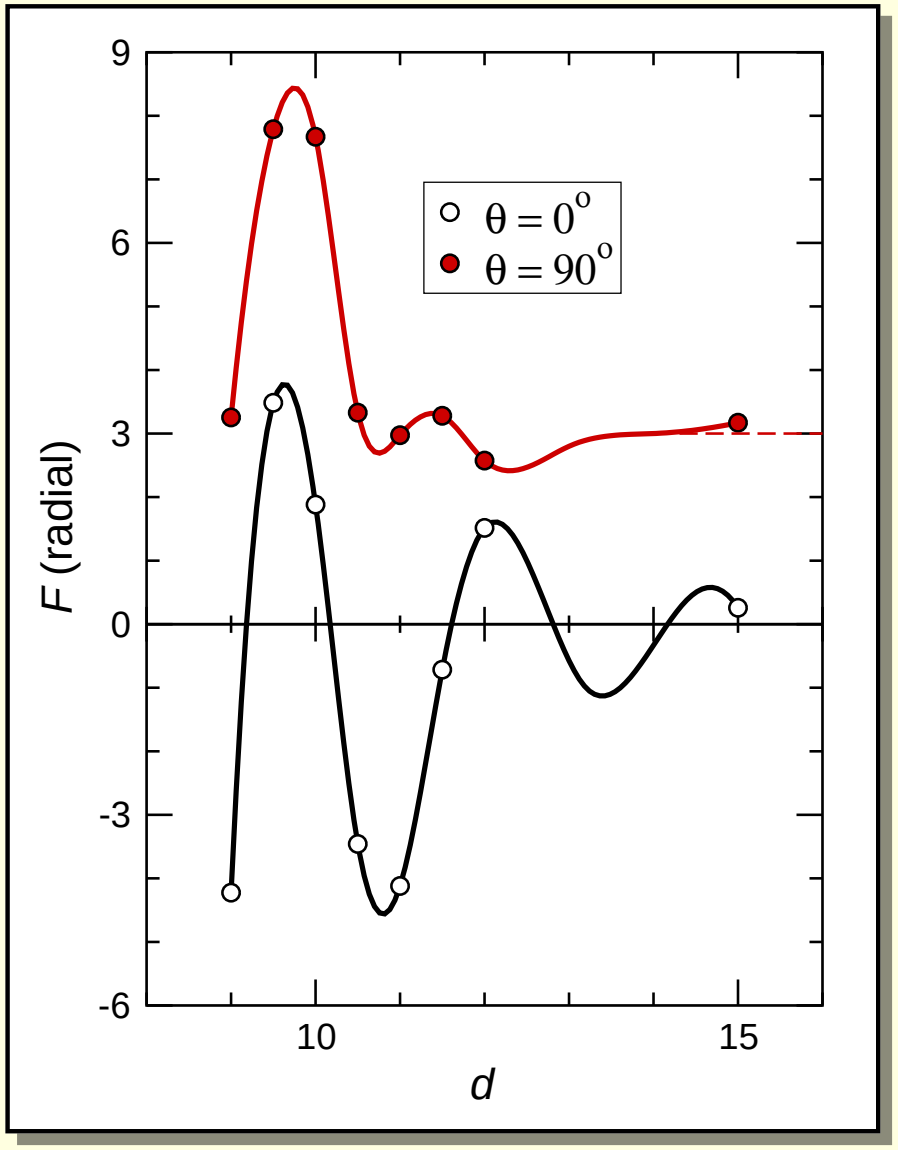

Tangential Force

- Component of force along tangential direction
  - ➥ perpendicular to line of centres
- Solvent effects at small separation
- Some hint of elastic behaviour at large separation
- Curves are a single-parameter fit (strength) to $\mathcal{U}$

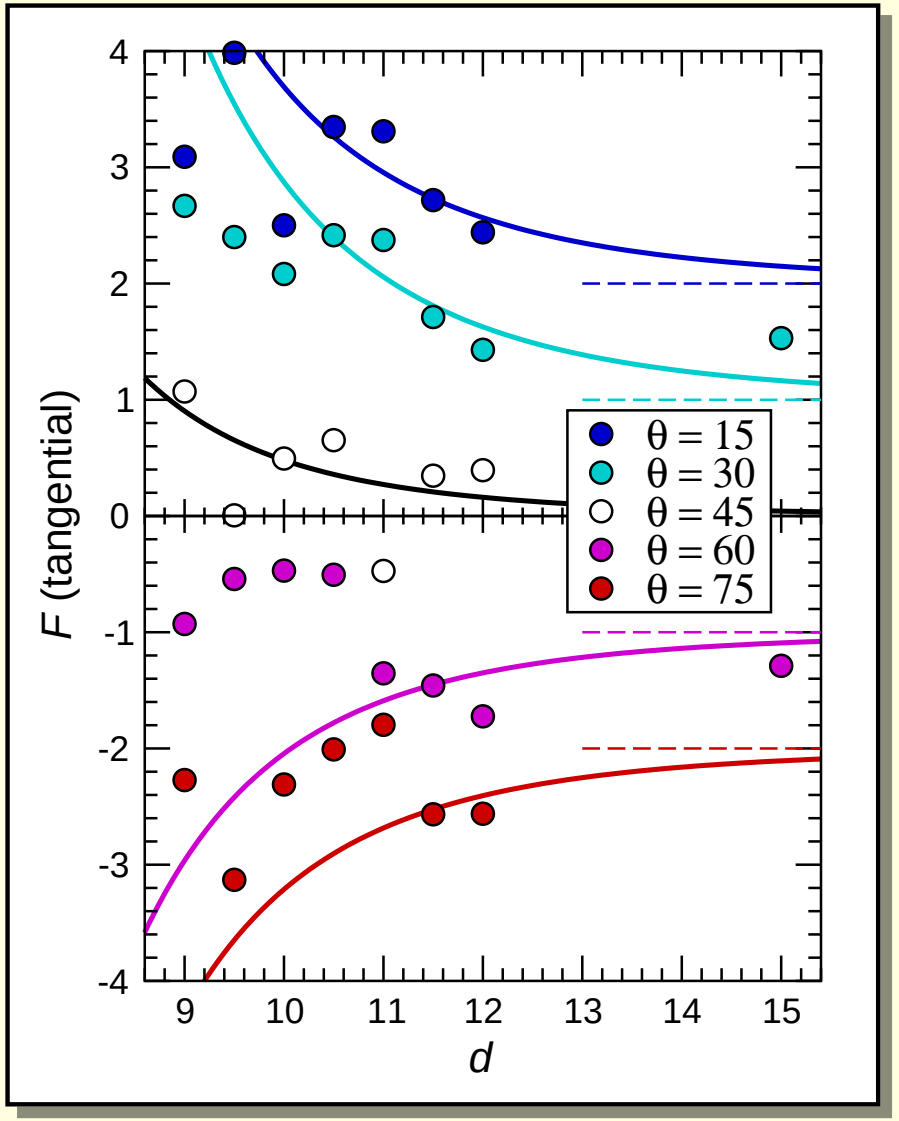

Acknowledgements

Colleagues

- M. S. Al-Barwani, A. J. McDonald, G. S. Sutcliffe
- G. Germano, F. Schmid, N. Akino, D. Andrienko

Advice

- R. Evans, R. van Roij, R. Roth, H. Lange

Hospitality

- K. Kremer, K. Binder

Funding

- Engineering and Physical Sciences Research Council
- Alexander von Humboldt foundation

References

[1] M. A. Glaser, R. Malzbender, N. A. Clark, and D. M. Walba. Atomic detail simulation studies of tilted smectics. *J. Phys. Cond. Mat.*, 6:A261–A268, 1994.

[2] E. Garcia, M. A. Glaser, N. A. Clark, and D. M. Walba. HFF: a force field for liquid crystal molecules. *J. Molec. Struc. - THEOCHEM*, 464:39–48, 1999.

[3] S. J. Clark, C. J. Adam, G. J. Ackland, J. White, and J. Crain.

Properties of liquid crystal molecules from first principles computer simulation. *Liq. Cryst.*, 22:469–475, 1997.

[4] S. J. Clark, C. J. Adam, D. J. Cleaver, and J. Crain. Conformational energy landscapes of liquid crystal molecules. *Liq. Cryst.*, 22:477–482, 1997.

[5] D. L. Cheung, S. J. Clark, and M. R. Wilson. Parametrization and validation of a force field for liquid-crystal forming molecules. *Phys. Rev. E*, 65:051709, 2002.

[6] J. G. Gay and B. J. Berne. Modification of the overlap potential to mimic a linear site-site potential. *J. Chem. Phys.*, 74:3316–3319, 1981.

[7] E. de Miguel, L. F. Rull, M. K. Chalam, and K. E. Gubbins. Liquid-vapor coexistence of the Gay-Berne fluid by Gibbs

ensemble simulation. *Molec. Phys.*, 71:1223–1231, 1990.

[8] R. Berardi, A. P. J. Emerson, and C. Zannoni. Monte Carlo investigations of a Gay-Berne liquid crystal. *J. Chem. Soc. Faraday Trans.*, 89:4069–4078, 1993.

[9] E. de Miguel, E. Martín del Río, J. T. Brown, and Michael P. Allen. Effect of the attractive interactions on the phase behavior of the Gay-Berne liquid crystal model. *J. Chem. Phys.*, 105:4234–4249, 1996.

[10] J. T. Brown, Michael P. Allen, E. Martín del Río, and E. de Miguel. Effects of elongation on the phase behavior of the Gay-Berne fluid. *Phys. Rev. E*, 57:6685–6699, 1998.

[11] R. Berardi, C. Fava, and C. Zannoni. A generalized Gay-Berne intermolecular potential for biaxial particles. *Chem. Phys. Lett.*,

236:462–468, 1995.

[12] P. J. Camp and Michael P. Allen. Phase diagram of the hard biaxial ellipsoid fluid. *J. Chem. Phys.*, 106:6681–6688, 1997.

[13] P. J. Camp, Michael P. Allen, and A. J. Masters. Theory and computer simulation of bent-core molecules. *J. Chem. Phys.*, 111:9871–9881, 1999.

[14] J. S. van Duijneveldt and Michael P. Allen. Computer simulation study of a flexible-rigid-flexible model for liquid crystals. *Molec. Phys.*, 92:855–870, 1997.

[15] Alexey V. Lyulin, Muataz S. Al-Barwani, Michael P. Allen, Mark R. Wilson, Igor Neelov, and Nicholas K. Allsopp. Molecular dynamics simulation of main chain liquid crystalline polymers. *Macromolecules*, 31:4626–4634, 1998.

[16] J. S. van Duijneveldt, A. Gilvillegas, G. Jackson, and Michael P. Allen. Simulation study of the phase behavior of a primitive model for thermotropic liquid crystals: Rodlike molecules with terminal dipoles and flexible tails. *J. Chem. Phys.*, 112:9092–9104, 2000.

[17] R. Berardi, M. Fehervari, and C. Zannoni. A monte carlo simulation study of associated liquid crystals. *Molec. Phys.*, 97:1173–1184, 1999.

[18] C. Oseen. Theory of liquid crystals. *Trans. Faraday Soc.*, 29:883–899, 1933.

[19] F. C. Frank. On the theory of liquid crystals. *Discuss. Faraday Soc.*, 25:19–28, 1958.

[20] P. G. de Gennes and J. Prost. *The Physics of Liquid Crystals*.

Clarendon Press, Oxford, second, paperback edition, 1995.

[21] L. Onsager. The effects of shape on the interaction of colloidal particles. *Ann. N. Y. Acad. Sci.*, 51:627, 1949.

[22] R. Evans. *Adv. Phys.*, 28:143, 1979.

[23] R. Evans. Microscopic theories of simple fluids and their interfaces. In J. Charvolin, J. F. Joanny, and J. Zinn-Justin, editors, *Liquids at Interfaces*, pages 1–98, Amsterdam, 1989. Elsevier Science Publishers B.V. Les Houches, Session XLVIII 1988.

[24] R. Evans. Density functionals in the theory of nonuniform fluids. In D. Henderson, editor, *Fundamentals of Inhomogeneous Fluids*, chapter 3, pages 85–175. Dekker, New York, 1992.

[25] V. V. Ginzburg, M. A. Glaser, and N. A. Clark. Liquid crystal

phase diagram of the Gay-Berne fluid by density functional theory. *Liq. Cryst.*, 23:227–234, 1997.

[26] J. D. Parsons. *Phys. Rev. A*, 19:1225, 1979.

[27] S.-D. Lee. A numerical investigation of nematic ordering based on a simple hard-rod model. *J. Chem. Phys.*, 87:4972–4974, 1987.

[28] S.-D. Lee. The Onsager-type theory for nematic ordering of finite-length hard ellipsoids. *J. Chem. Phys.*, 89:7036–7037, 1989.

